Electronic Supplementary Information (ESI) for

π-Extended Nonplanar Cobalt Porphyrins Immobilized on MWCNTs as Efficient Electrocatalysts for Selective Oxygen Reduction Reaction

Amir Sohel Bulbul,[a] Vikram Rathour,[b] Vellaichamy Ganesan,[b] and Muniappan Sankar[a,*]

[a]*Department of Chemistry, Indian Institute of Technology Roorkee, Roorkee-247667, India*
[b]*Department of Chemistry, Institute of Science, Banaras Hindu University, Varanasi-221005, India*

Table of Contents

EXPERIMENTAL SECTION:

Chemicals and Instruments

Benzaldehyde and Pyrrole were purchased from SRL India and TCI Chemicals, respectively. Metal salts, K_2CO_3 were purchased from Himedia, India. $TBAPF_6$, N-bromosuccinimide (NBS), methylacrylate, and $Pd(OAc)_2$ were purchased from Alfa Aesar, SRL, TCI, and Loba Chemie respectively, and used as received. CH_2Cl_2 and toluene were purified and dried over P_2O_5 before use. HPLC grade dimethylformamide (DMF) was purchased from SRL India and used without further purification. Potassium hydroxide was purchased from Merck Life Science Private Limited, India. Multi-walled carbon nanotubes (MWCNT) was purchased from Adnano Technologies, India. N-bromosuccinimide was recrystallized from hot water and dried for 8 h at 70 °C under vacuum. $TBAPF_6$ was recrystallized twice from hot ethanol and dried under a vacuum. Silica gel (100-200 mesh) employed in this work for purification was purchased from Finar Chemicals, India and used as received. Precoated thin layer silica gel chromatographic plates were purchased from Merck and used as received. 2,3-Dichloro-5,6-dicyano-1,4-benzoquinone (DDQ) was obtained from sigma-aldrich.

The electronic absorption spectra were recorded on a Shimadzu spectrophotometer (UV-2600) using a pair of quartz cells of 10 mm path length and 3.5 mL volume. All the proton NMR spectra were recorded on a JEOL ECX 500 MHz using $CDCl_3$ as a solvent at 298 K. EPR spectra were recorded on a Bruker BIOSPIN EMXmicro A200-9.5/12/S/W EPR spectrometer with X-band microwave source at 100 K. The X-ray quality single-crystals of $Co(Cl)TFPMB(VCN)_2$•CH_3OH were obtained by slow diffusion of methanol into the saturated porphyrin solution in $CHCl_3$. The single-crystal X-ray diffraction data were collected on a Bruker APEX4 D8 QUEST Photon III C7 diffractometer. The MALDI-TOF mass spectra were recorded on Bruker UltrafleXtreme-TN MALDI-TOF mass spectrometer in a positive ion mode. The cyclic voltammetry (CV) studies were carried out using CH instruments (CHI 7044E). A three-electrode assembly was used that consisted of a platinum working electrode, Ag/AgCl as a reference electrode, and Pt wire as a counter electrode. The porphyrin concentration was maintained at ~1 mM during electrochemical measurements. The whole

experiment was performed under an inert atmosphere. Oxygen reduction reaction (ORR) studies were done with the three-electrode system using CHI-660 C (CH Instruments, USA) and the rotation of the electrode was regulated by a modulated speed rotator (Pine research instrument, USA). In these studies, platinum wire was used as the counter electrode, saturated calomel electrode ($Hg/HgCl_2$) was used as the reference electrode, and glassy carbon (GC) electrode with geometrical surface area 0.071 cm^2 or GC rotating disc electrodes (GC_{RDE}) with a geometrical surface area of 0.196 cm^2 are used as the working electrode. The working electrode was cleaned by rubbing on a wet Buehler-felt pad with 0.05 micron neutral alumina powder, then rinsing with water and sonicating for 20 s. Catalyst ink was prepared by dispersing 5 mg of the respective materials in 500 µL of DMF, followed by sonicating it for 1 h. The working electrodes were prepared by coating 5 µL on the GC and 14 µL on $GC_{RDE.}$ The observed electrode potential ($E_{Hg/HgCl2}$) was converted to a reversible hydrogen (RHE) potential by the equation, $E_{RHE} = E_{Hg/HgCl2} + 0.0591 \times pH + 0.241$.[S1] ORR studies were done by CV and linear sweep voltammetry (LSV) in 0.1 M KOH under the argon and oxygen saturated environments. CV response was recorded in static conditions in the potential range of -0.4 to 0.6 V *vs.* SCE with a scan rate of 20 mV/s. LSV was measured with the materials coated on GC_{RDE} under the hydrodynamic condition at a rotation rate of 1600 rpm with a scan rate of 10 mV/s. K-L (Koutecky-Levich) equation (Equations S1 and S2) was used to calculate the number of electrons transferred per oxygen molecule during ORR.[S2]

$$\frac{1}{J} = \frac{1}{J_K} + \frac{1}{J_L} = \frac{1}{B\omega^{1/2}} + \frac{1}{j_k} \qquad \text{S1}$$

$$B = 0.62nFC_O(D_0)^{2/3}\,\Upsilon^{-1/6} \qquad \text{S2}$$

Where J, J_K, and J_L denote the current density, kinetic limiting current density, and diffusion limiting current density respectively, ω is the angular velocity of the electrode, n is the number of electrons transferred per O_2 molecule, F is the Faraday constant (96500 C mol^{-1}), C_O is the concentration of O_2 (1.2×10^{-6} mol cm^{-3}), D_0 is the diffusion coefficient of O_2 ($1.9 \times 10^{-5} cm^2 s^{-1}$), and Υ is the kinematic viscosity of the electrolyte (0.01 $cm^2 s^{-1}$) respectively. The field emission scanning electron microscopy (FESEM) images were obtained from FESEM (Apreo S Low Vac model) with the advanced EDAX detector. High-resolution transmission electron microscopy (HR-TEM) images and selected area electron diffraction (SAED) patterns were recorded by 300 kV JEM-3200FS field emission electron microscope. X-ray photoelectron spectra (XPS) were recorded using PHI 5000 VersaProbe III scanning micro-focused X-ray beam. Powder X-ray diffraction (XRD) patterns were recorded using a BRUKER D8 advance

X-Ray diffractometer (Cu-Kα radiation (0.1541 nm)). Raman spectra were recorded using RENISHAW inVia Raman Microscope, GL12 8JR, United Kingdom.

Free-base porphyrins H_2TPP, H_2DFP(VCN)$_2$, and H_2TPP(NO_2)MB were synthesised according to the modified literature method.[S3–S5] The investigated porphyrins, CoTPP (**1Co**), CoDFP(VCN)$_2$ (**2Co**) were prepared according to Scheme 1 and CoTFPMB(VCN)$_2$ (**3Co**) was prepared as per the synthetic strategy presented in Scheme 2.

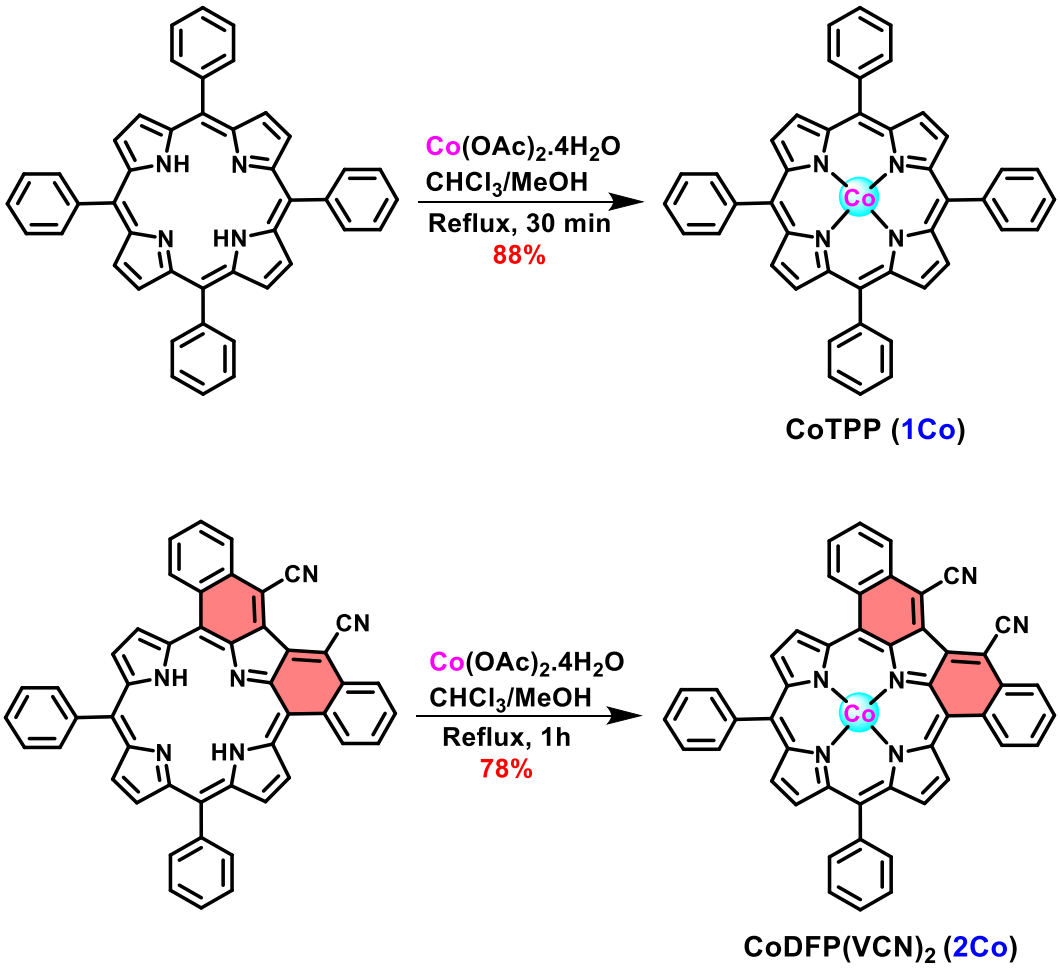

Scheme 1 Synthesis of **1Co** and **2Co**.

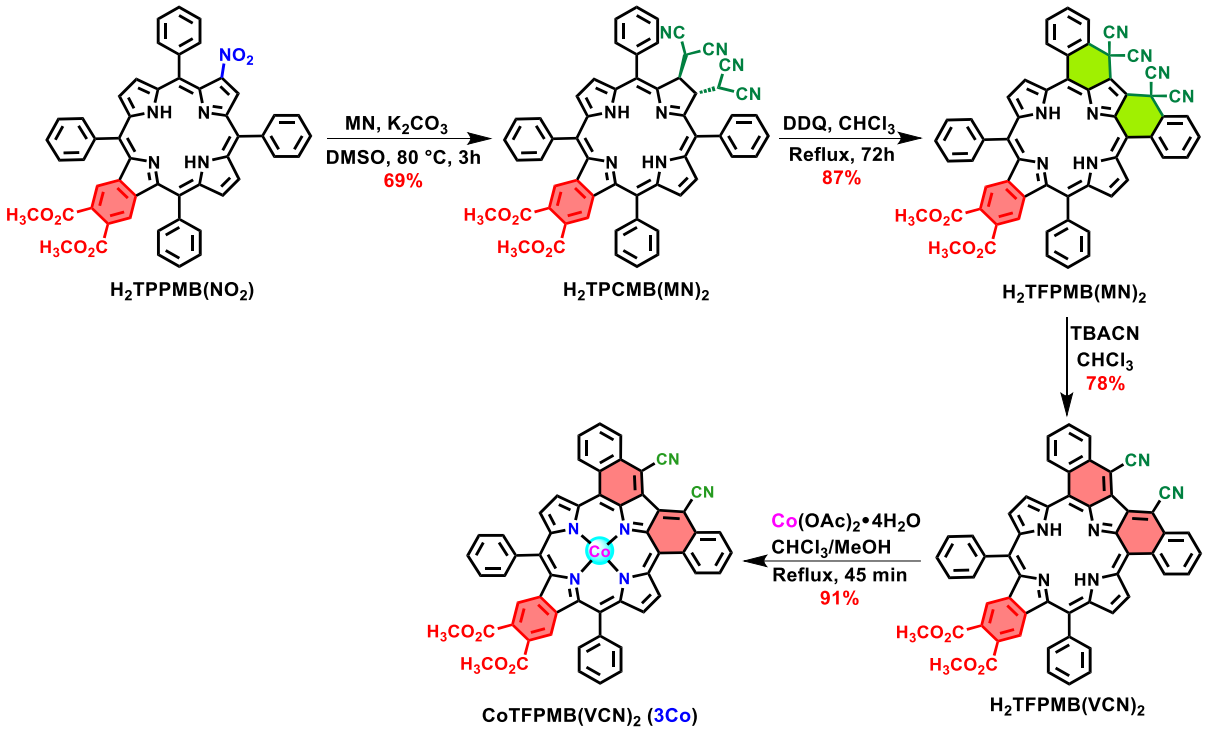

Scheme 2 Synthetic strategy for **3Co**.

Synthesis of CoTPP (1Co): A 30 mg of free base porphyrin, H_2TPP was dissolved in 10 mL of $CHCl_3$. To this, 10 equiv. of $Co(OAc)_2•4H_2O$ in 2 mL of MeOH solution was added and the resulting mixture was refluxed for 30 min. The organic layer was washed with water and reduced under pressure. The crude product was purified by column chromatography using $CHCl_3$ as an eluent.

1Co Yield: 88 % (29 mg, 0.043 mmol) UV/vis (CH_2Cl_2): λ_{max} (nm) ($\varepsilon \times 10^{-3}$ L $mol^{-1}cm^{-1}$): 409 (244), 528 (183). ^1H NMR (500 MHz, $CDCl_3$) δ(ppm): 16.02 (s, 8H, β-H), 13.20 (s, 8H, *meso-o*-Ph-H), 9.96-9.75 (m, 12H, *meso-m,p*-Ph-H). MALDI-TOF-MS. Found: m/z 671.320 ($[M]^+$) Calcd: m/z 671.165. Elemental analysis for $C_{44}H_{28}N_4Co$: C, 78.68; H, 4.20; N, 8.34. Found: C, 78.59; H, 4.24; N, 8.29.

Synthesis of di-fused porphyrin, $CoDFP(VCN)_2$ (2Co): A 30 mg of free base di-fused porphyrin $H_2DFP(VCN)_2$ was dissolved in 12 mL of $CHCl_3$. To this, a methanolic solution of $Co(OAc)_2•4H_2O$ (10 equiv.) was added and the resulting mixture was refluxed for 1 h. The organic layer was washed with water three times and the solvent was removed under pressure. The crude product was purified by column chromatography using $CHCl_3$ as an eluent.

2Co Yield: 78 % (25 mg, 0.033 mmol) UV/vis (CH_2Cl_2): λ_{max} (nm) ($\varepsilon \times 10^{-3}$ L $mol^{-1}cm^{-1}$): 340 (69), 418 (120), 496 (55), 723 (22), 796 (37). ^{1}H NMR (500 MHz, $CDCl_3$) δ(ppm): 10.0-8.52 (m, 14H, β-H & fused Ph-H), 7.92-7.69 (m, 10H, unfused *meso*-Ph-H). MALDI-TOF-MS. Found: m/z 743.250 ($[M]^+$) Calcd: m/z 743.139. Elemental analysis for $C_{48}H_{24}N_6Co$: C, 77.52; H, 3.25; N, 11.30. Found: C, 77.49; H, 3.28; N, 11.35.

Synthesis of *trans*-monobenzochlorin H_2TPCMB(MN)$_2$: K_2CO_3 (200 mg, 1.45 mmol) and malononitrile (81 μL, 1.44 mmol) were dissolved in 3 mL of DMSO and stirred for 15 min under argon purging. To this, 120 mg (0.145 mmol) $H_2TPP(NO_2)MB$ was added and the resulting mixture was stirred at 80 °C for 3 h. The progress of the reaction was monitored by UV-Vis spectroscopy and TLC. After completion, the reaction mixture was allowed to raise to room temperature and diluted by adding 10 mL of $CHCl_3$. The diluted reaction mixture was washed three times with brine solution. The organic layer was separated and dried over anhydrous Na_2SO_4. The solvent was removed under reduced pressure and the desired product was chromatographed using $CHCl_3$ as eluent and recrystallized by $CHCl_3$/MeOH (3:1) mixture.

H_2TPCMB(MN)$_2$ Yield: 69% (91 mg, 0.099 mmol), UV/vis (CH_2Cl_2): λ_{max} (nm) ($\varepsilon \times 10^{-3}$ L $mol^{-1}cm^{-1}$): 407(sh) (200), 428 (891), 516 (52), 558 (12), 610 (19), 666 (92). ^{1}H NMR (500 MHz, $CDCl_3$) δ(ppm): 8.69 (d, J = 4.8 Hz, 2H, β-H), 8.34 – 8.30 (m, 4H, *meso*-Ph-H), 8.23 (d, J = 7.4 Hz, 2H, *β*-H), 7.95 – 7.78 (m, 16H, *meso*-Ph-H), 7.24 (s, 2H, Benzo-CH), 5.38 (d, J = 4.0 Hz, 2H, β-CH Chlorin), 4.34 (d, J = 3.9 Hz, 2H, CH Chlorin), 3.88 (s, 6H, -$COOCH_3$), -2.12 (s, 2H, Inner NH). MALDI-TOF-MS. Found: m/z 911.109 ($[M+H]^+$) Calcd: m/z 911.302. Elemental analysis for $C_{58}H_{38}N_8O_4$: C, 76.47; H, 4.20; N, 12.30. Found: C, 76.41; H, 4.12; N, 12.36.

Oxidative fusion of *trans*-monobenzochlorin H_2TPCMB(MN)$_2$ to tri-fused monobenzoporphyrin, H_2TFPMB(MN)$_2$: An 80 mg of H_2TPCMB(MN)$_2$ was dissolved in 20 mL of $CHCl_3$. To this, 10 equiv. of DDQ was added and the resulting mixture was refluxed for 72 h. After completion, the reaction mixture was washed three times with water to remove excess DDQ. The organic layer was passed over anhydrous sodium sulfate and the solvent was evaporated under reduced pressure. The crude product was purified by silica gel column chromatography using $CHCl_3$ as an eluent.

H_2TFPMB(MN)$_2$ Yield: 87% (69 mg, 0.076 mmol), UV/vis (CH_2Cl_2): λ_{max} (nm) ($\varepsilon \times 10^{-3}$ L $mol^{-1}cm^{-1}$): 486 (619), 582 (39), 631 (13), 663 (15), 730 (39). ^{1}H NMR (500 MHz, $CDCl_3$) δ(ppm): 9.55 (d, J = 4.9 Hz, 2H, β-H), 8.77 (d, J = 4.9 Hz, 2H, β-H), 8.58 (d, J = 7.8 Hz, 2H,

Fused-*o*-Ph-H), 8.32 (d, *J* = 7.9 Hz, 2H, Fused-*p*-Ph-H), 8.06 (d, *J* = 7.3 Hz, 4H, Fused-*m*-Ph-H), 7.89 (dq, *J* = 25.7, 7.6 Hz, 8H, Unfused-*meso*-Ph-H), 7.74 (t, *J* = 7.6 Hz, 2H, Unfused-*meso*-Ph-H), 7.24 (s, 2H, Benzo-CH), 3.90 (s, 6H, -$COOCH_3$), -0.31 (s, 2H, Inner NH). ^{13}C NMR (126 MHz, $CDCl_3$) δ(ppm) 168.01, 150.59, 143.85, 141.95, 140.13, 139.97, 138.20, 135.42, 134.70, 133.23, 132.38, 130.07, 129.57, 129.22, 128.78, 128.40, 127.51, 127.16, 126.61, 120.27, 113.97, 111.22, 52.54, 36.84, 30.91, 29.71. MALDI-TOF-MS. Found: m/z 905.873 ($[M+H]^+$) Calcd: m/z 905.258. Elemental analysis for $C_{58}H_{32}N_8O_4$: C, 76.98; H, 3.56; N, 12.38. Found: C, 77.03; H, 3.51; N, 12.35.

Anion induced synthesis of H_2TFPMB(VCN)$_2$: A 40 mg (0.044 mmol) of H_2TFPMB(MN)$_2$ was dissolved in 10 mL of distilled $CHCl_3$. To this, 5 equiv. (0.221 mmol) tetrabutylammonium cyanide (TBACN) was added and stirred for 20 min at room temperature. The course of the reaction was monitored by UV-Vis spectroscopy and TLC. After completely consuming the precursor, the solution was washed three times with water. The organic layer was separated and dried over anhydrous Na_2SO_4. The solvent was removed under reduced pressure and the crude product was purified by silica gel column chromatography using $CHCl_3$ as eluent.

H_2TFPMB(VCN)$_2$ Yield: 78% (29 mg, 0.034 mmol), UV/vis (CH_2Cl_2): λ_{max} (nm) (ε × 10^{-3} L $mol^{-1}cm^{-1}$): 344 (36), 363 (36), 434 (99), 480 (40), 518 (49), 754 (14), 840 (26). ^1H NMR (500 MHz, $CDCl_3$) δ(ppm): 8.84 (dd, *J* = 16.3, 6.4 Hz, 4H, *β*-H & Fused-*meso*-Ph-H), 8.71 (d, *J* = 8.0 Hz, 2H, Fused-*meso*-Ph-H), 8.22 (d, *J* = 4.7 Hz, 2H, *β*-H), 7.94 (d, *J* = 7.5 Hz, 4H, Fused-*meso*-Ph-H), 7.85 (ddd, *J* = 30.3, 15.1, 7.6 Hz, 8H, Unfused-*meso*-Ph-H), 7.73 (t, *J* = 7.4 Hz, 2H, Unfused-*meso*-Ph-H), 7.07 (s, 2H, Benzo-CH), 3.89 (s, 6H, -$COOCH_3$). ^{13}C NMR (126 MHz, $CDCl_3$) δ(ppm): 168.28, 142.06, 140.08, 139.83, 135.88, 133.14, 132.62, 129.17, 128.85, 128.66, 128.55, 128.32, 127.44, 127.01, 125.78, 125.25, 116.31, 108.51, 106.34, 52.48, 29.70. MALDI-TOF-MS. Found: m/z 853.752 ($[M+H]^+$) Calcd: m/z 853.249. Elemental analysis for $C_{56}H_{32}N_6O_4$: C, 78.86; H, 3.78; N, 9.85. Found: C, 78.65; H, 3.70; N, 9.89.

Synthesis of tri-fused porphyrin, CoTFPMB(VCN)$_2$ (3Co): A 25 mg of free base trifused porphyrin H_2TFPMB(VCN)$_2$ was dissolved in 10 mL of $CHCl_3$. To this methanolic solution of $Co(OAc)_2$•$4H_2O$ (10 equiv.) was added and the resulting mixture was refluxed for 45 min. The organic layer was washed with water three times and the solvent was removed under pressure. The crude product was purified by column chromatography using acetone: $CHCl_3$ (1:99) as eluent.

3Co Yield: 91 % (24 mg, 0.026 mmol) UV/vis (CH_2Cl_2): λ_{max} (nm) (ε × 10^{-3} L $mol^{-1}cm^{-1}$): 331 (41), 445 (72), 526 (43), 763 (12), 851 (20). ^1H NMR (500 MHz, $CDCl_3$) δ(ppm): 8.53 (s, br,

12H, β-H & fused Ph-H), 7.84 (s, br, 10H, unfused Ph-H), 7.07 (s, 2H, benzo-CH), 3.87 (s, br, 6H, -$COOCH_3$). MALDI-TOF-MS. Found: m/z 909.365 ($[M]^+$) Calcd: m/z 909.166. Elemental analysis for $C_{56}H_{30}N_6O_4Co$: C, 73.93; H, 3.32; N, 9.24. Found: C, 73.98; H, 3.27; N, 9.31.

General procedure for the preparation of nanocomposites (1Co@MWCNT, 2Co@MWCNT, and 3Co@MWCNT):

All the porphyrin adsorbed MWCNT nanocomposites were prepared according to the modified literature method.[S2] MWCNT (20 mg) and ~1 mM porphyrin in 20 mL of DMF were mixed and the resulting mixture was ultrasonicated for 30 min. Then the charged solutions were kept under stirring for 24 h at room temperature, followed by centrifugation and washed with DMF. The resulting materials were dried in a vacuum oven.

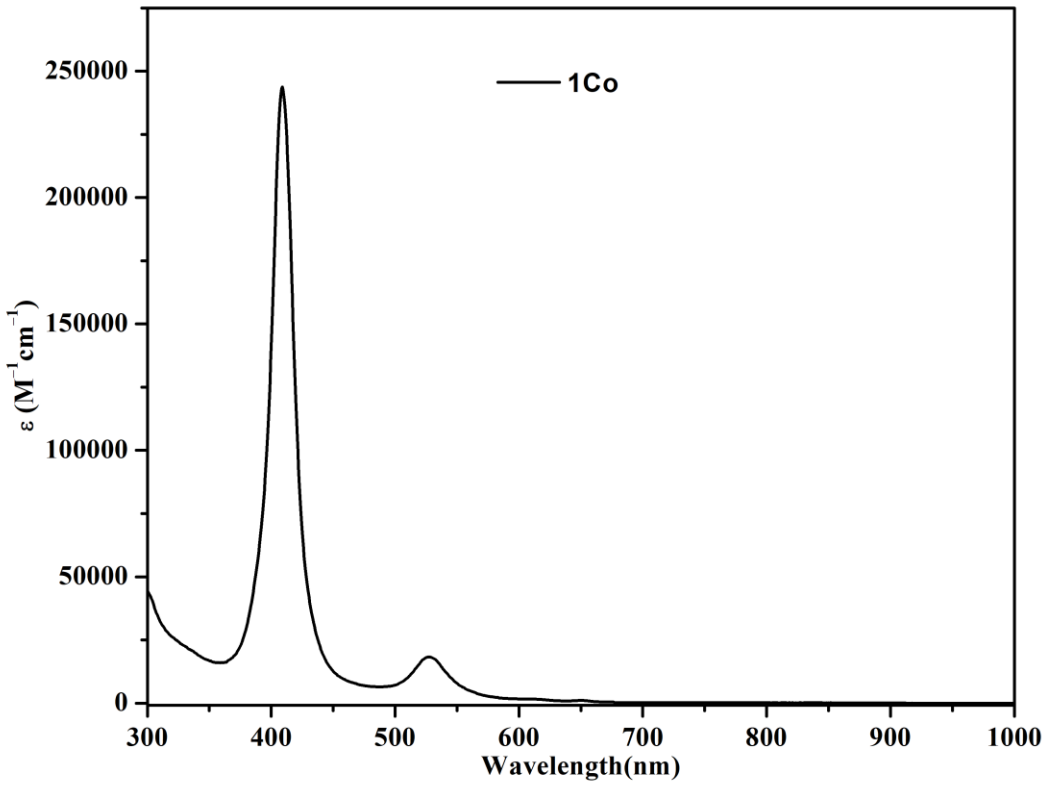

Fig. S1 UV-Vis Absorption Spectrum of **1Co** in CH_2Cl_2 at 298 K.

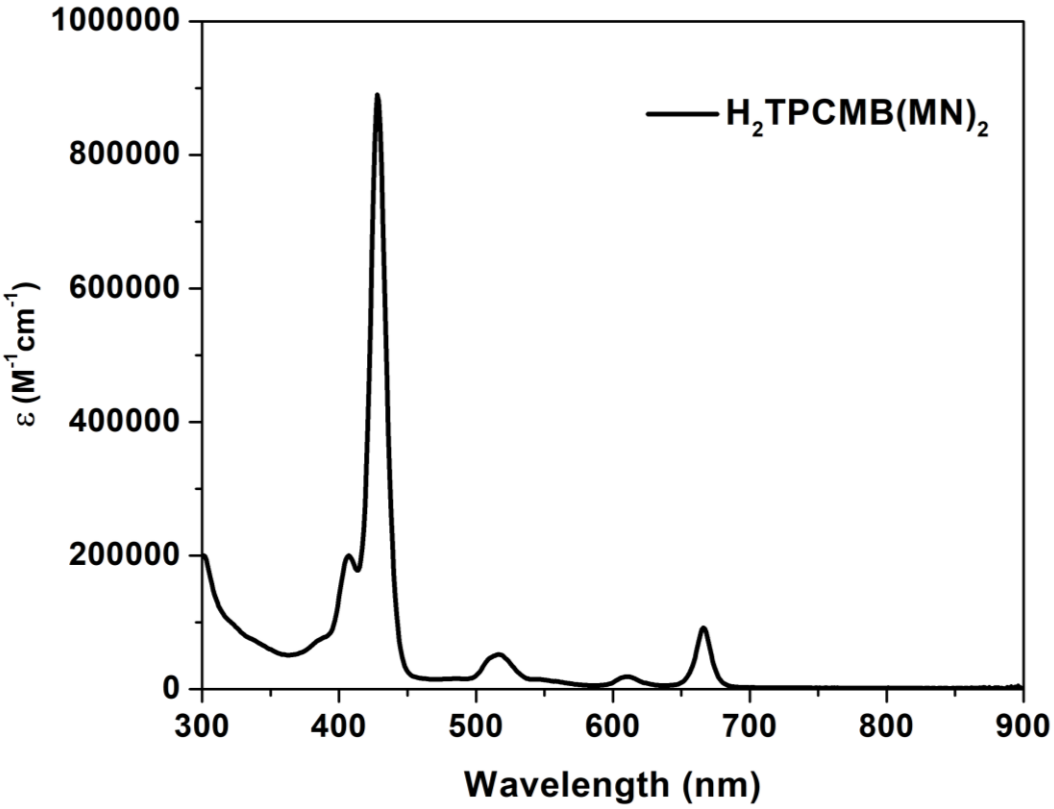

Fig. S2 UV-Vis Absorption Spectrum of H_2TPCMB(MN)$_2$ in CH_2Cl_2 at 298 K.

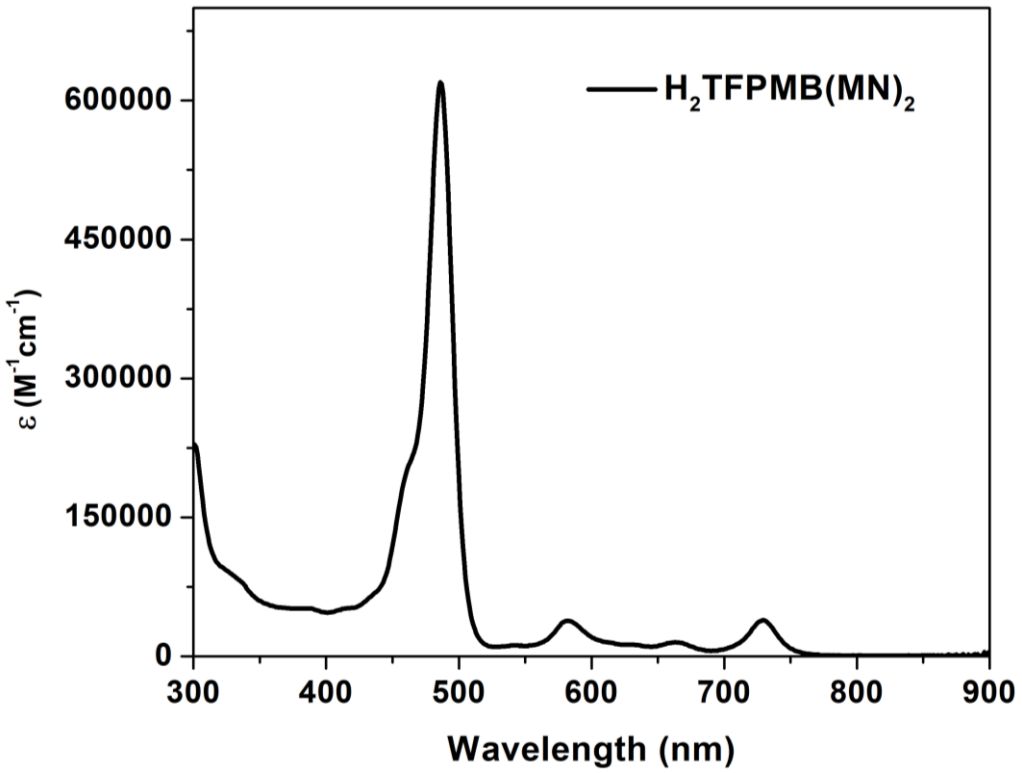

Fig. S3 UV-Vis Absorption Spectrum of H_2TFPMB(MN)$_2$ in CH_2Cl_2 at 298 K.

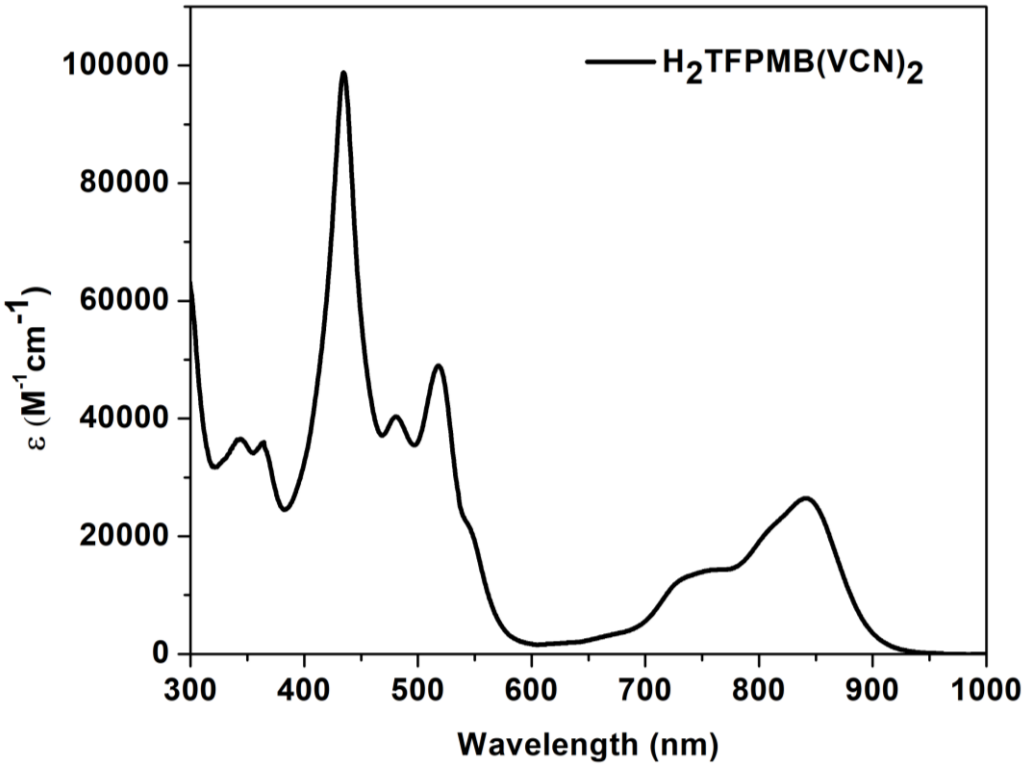

Fig. S4 UV-Vis Absorption Spectrum of H_2TFPMB(VCN)$_2$ in CH_2Cl_2 at 298 K.

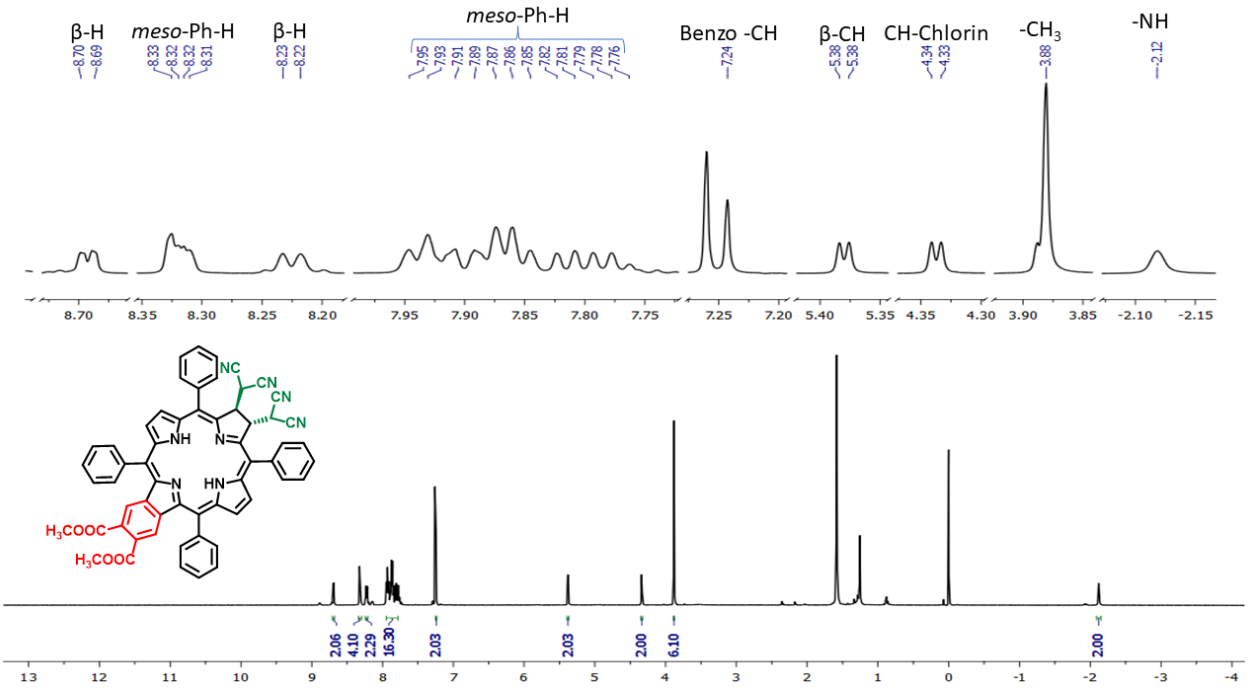

Fig. S5 ^{1}H NMR Spectrum of H_2TPCMB(MN)$_2$ in $CDCl_3$ at 298 K.

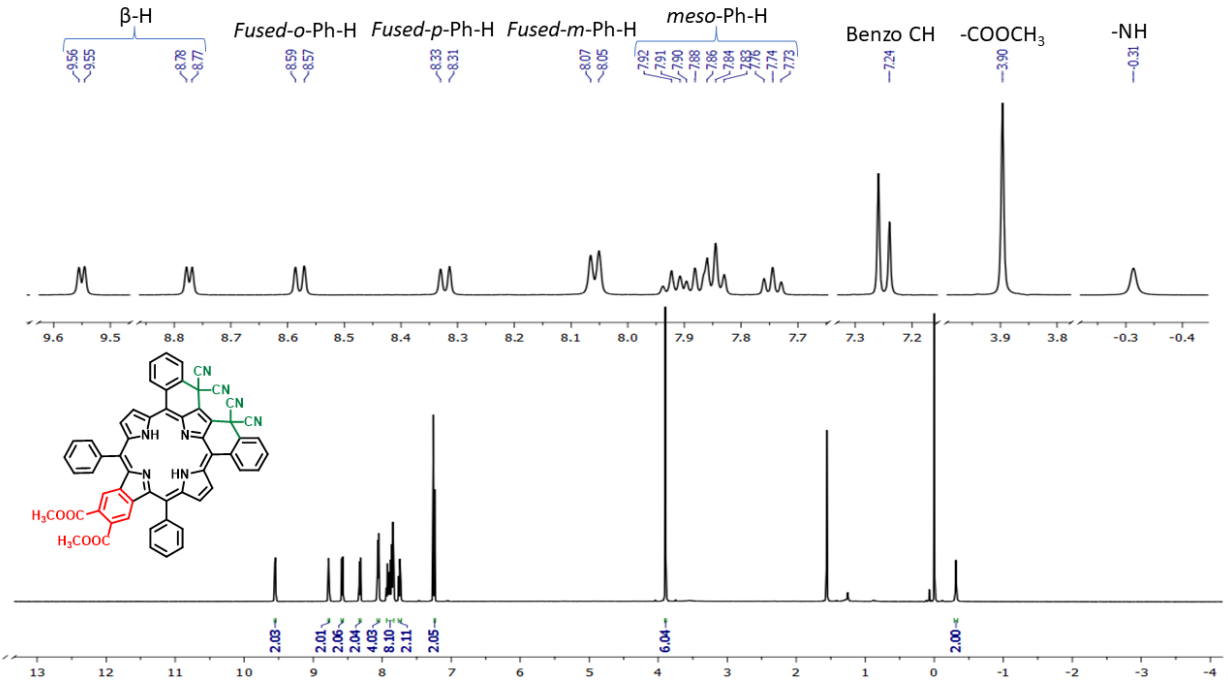

Fig. S6 ^{1}H NMR Spectrum of H_2TFPMB(MN)$_2$ in $CDCl_3$ at 298 K.

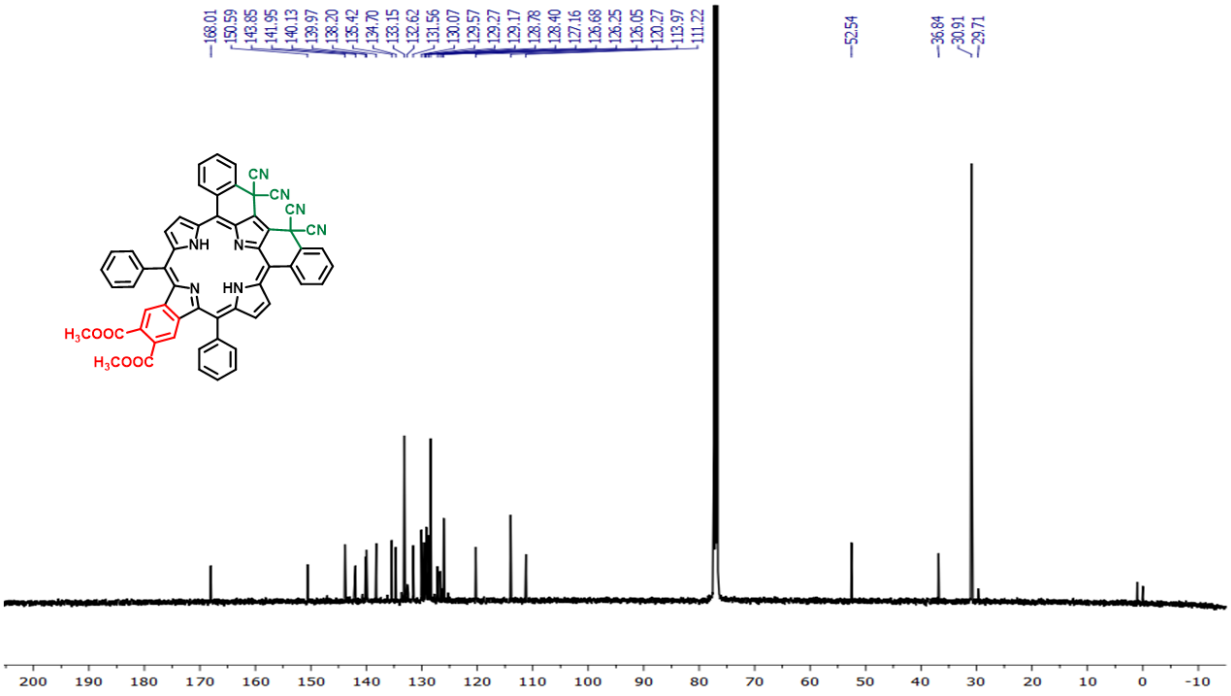

Fig. S7 ^{13}C NMR Spectrum of H_2TFPMB(MN)$_2$ in $CDCl_3$ at 298 K.

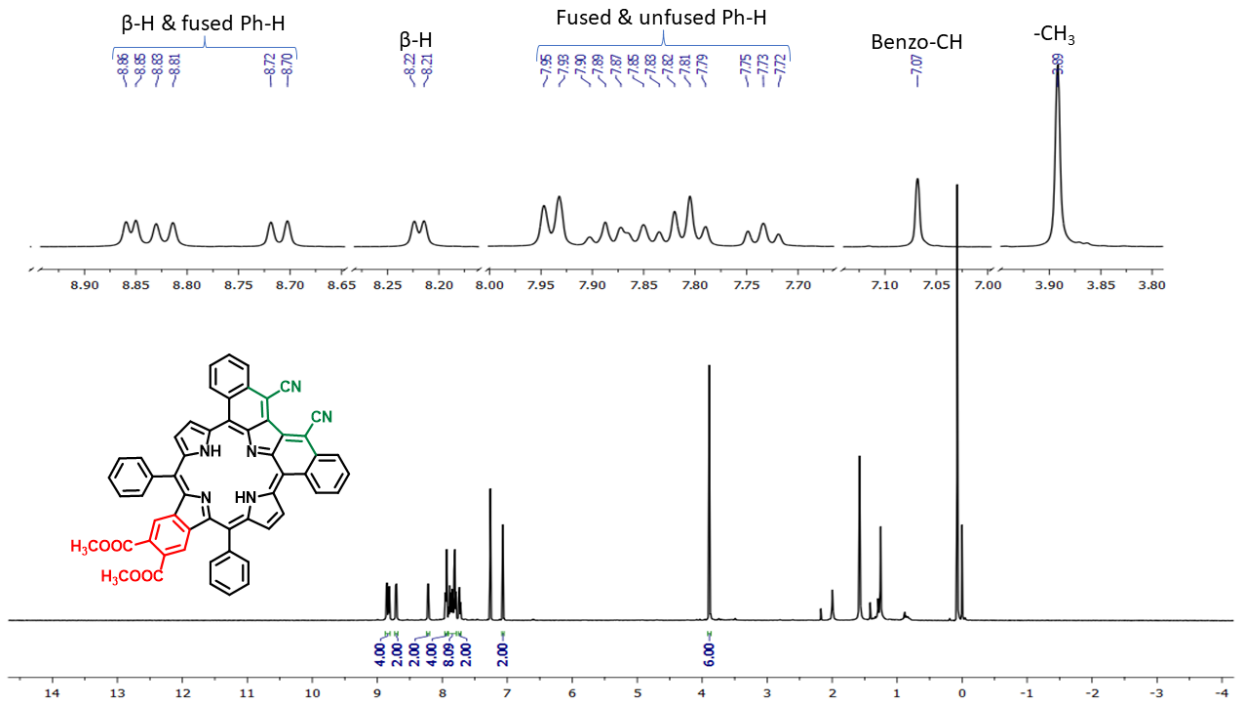

Fig. S8 ^{1}H NMR Spectrum of H_2TFPMB(VCN)$_2$ in $CDCl_3$ at 298 K.

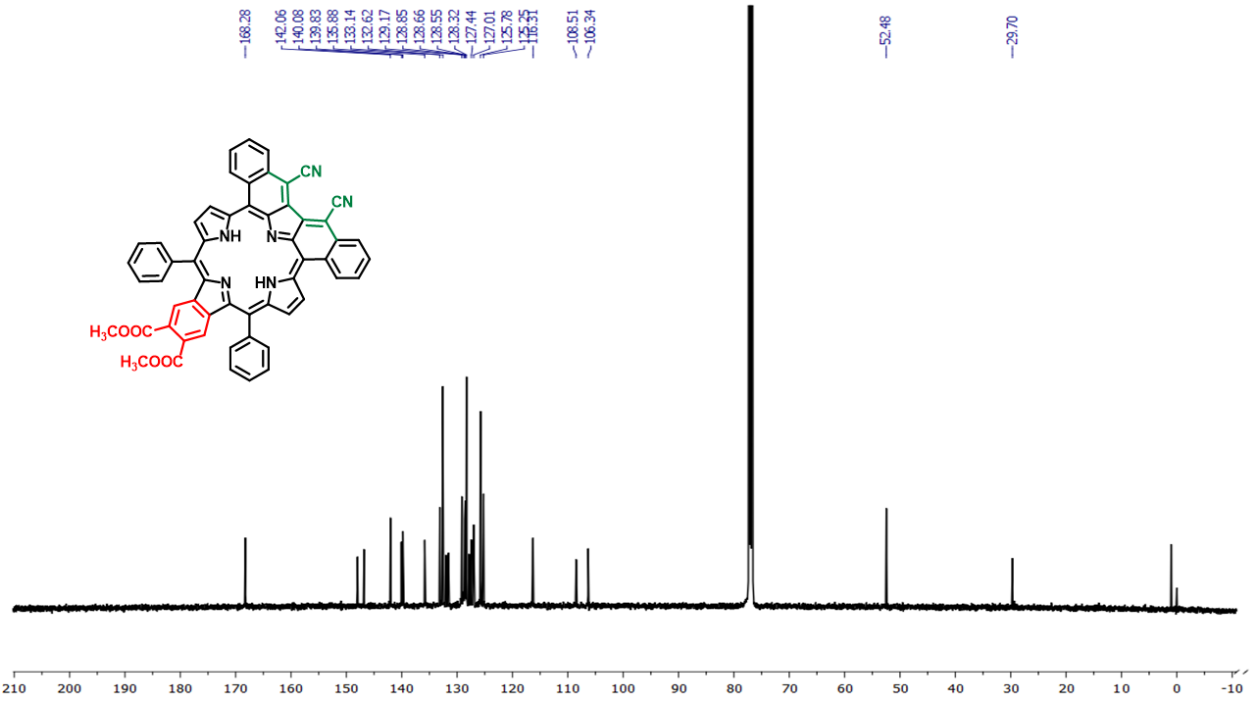

Fig. S9 ^{13}C NMR Spectrum of H_2TFPMB(VCN)$_2$ in $CDCl_3$ at 298 K.

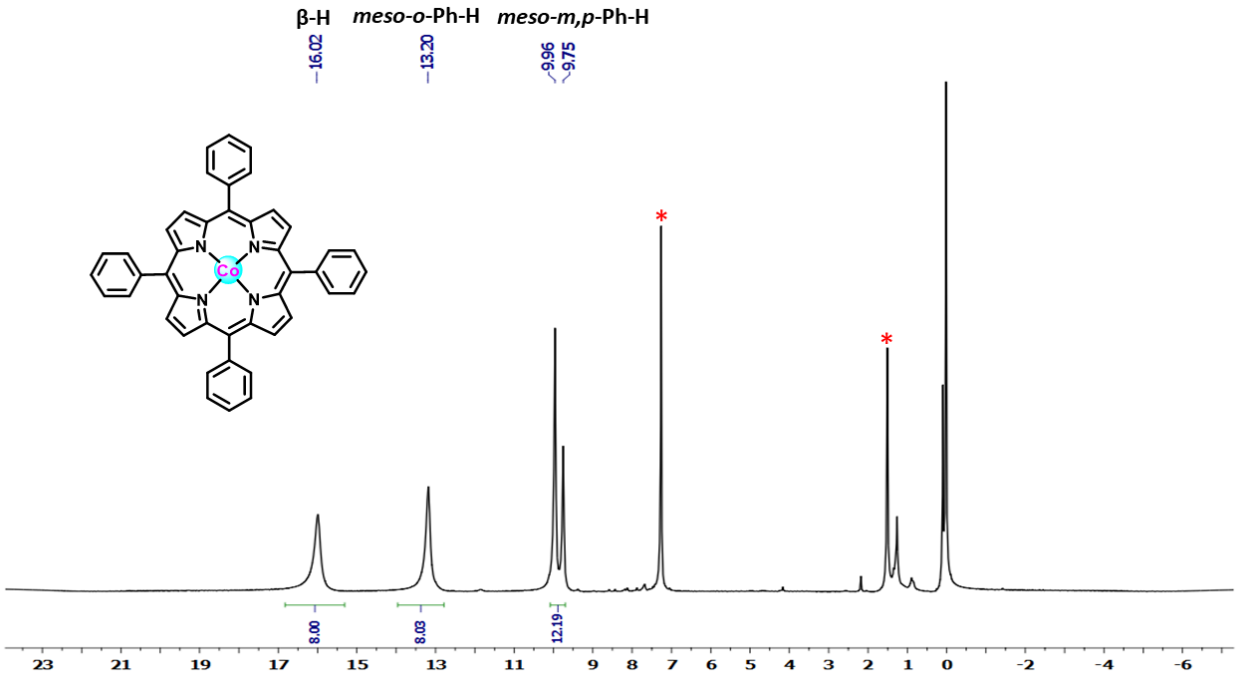

Fig. S10 ^{1}H NMR Spectrum of **1Co** in $CDCl_3$ at 298 K.

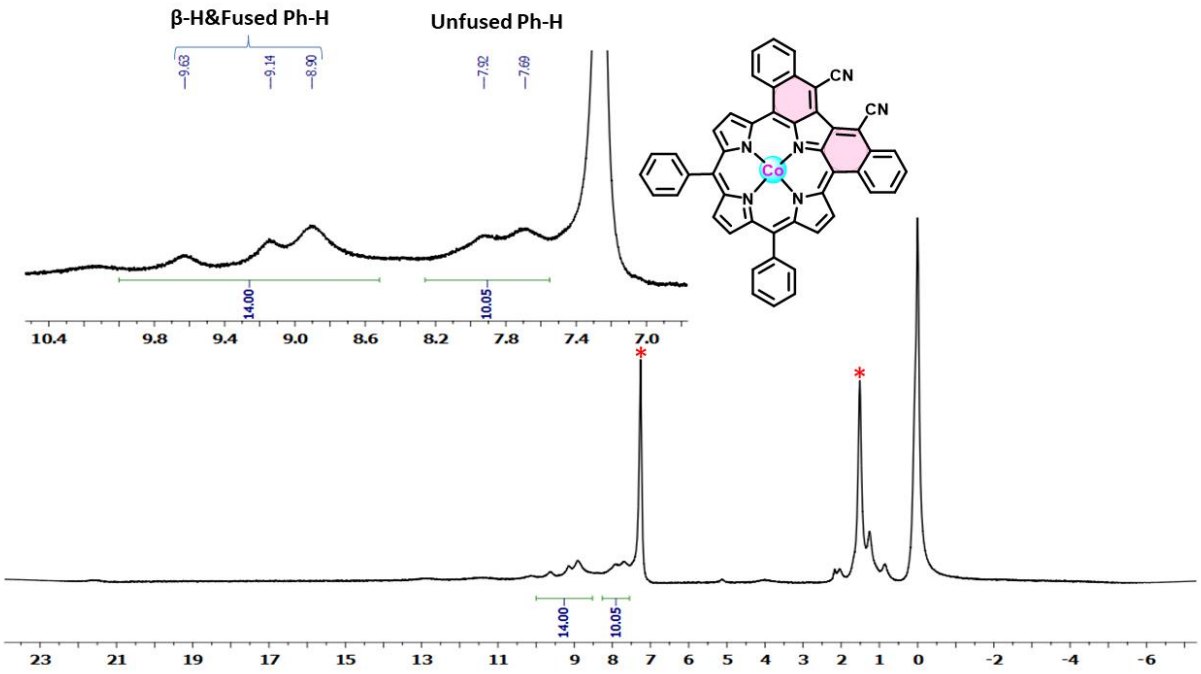

Fig. S11 ^{1}H NMR Spectrum of **2Co** in $CDCl_3$ at 298 K.

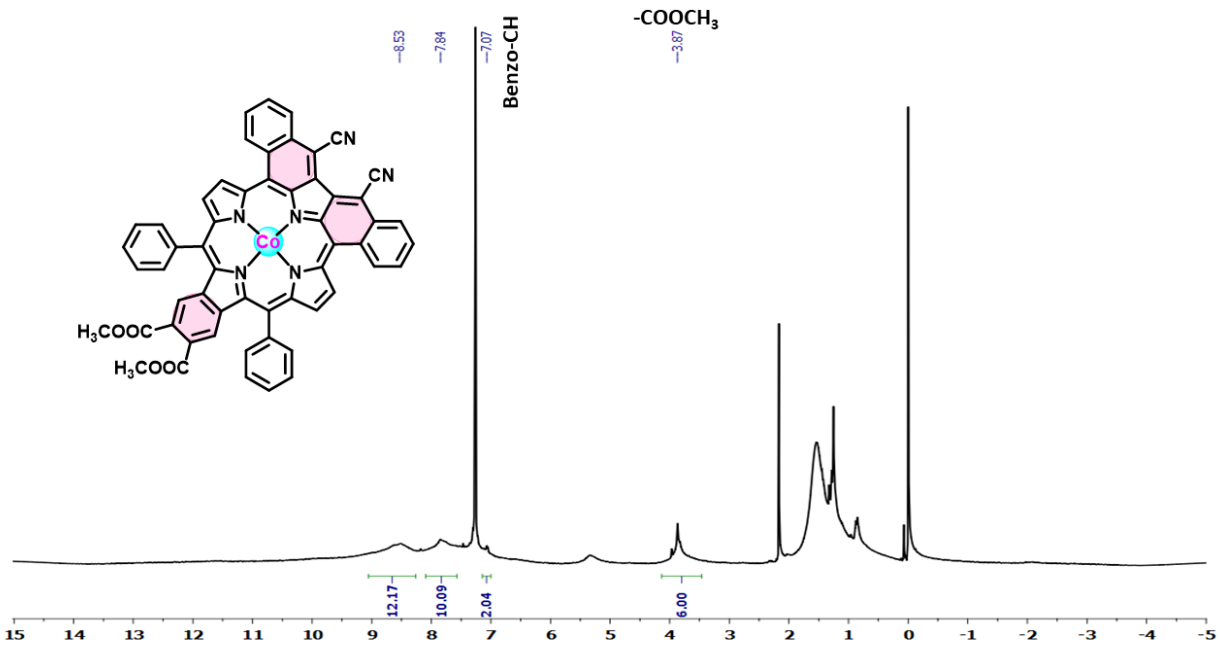

Fig. S12 ^{1}H NMR Spectrum of **3Co** in $CDCl_3$ at 298 K.

Electron paramagnetic resonance (EPR) Analysis: The X-band EPR analysis revealed that **2Co** and **3Co** are both EPR active in toluene whereas silent in $CHCl_3$ (Figs. S13 & S14). The Cl^- comes as contaminant from $CHCl_3$ due to its high affinity towards the Co.[S6] It was further supported by the NMR analysis, where all the signals of **2Co** and **3Co** resonate in the typical region (Figs. S11 & S12). In addition, the XPS analysis unequivocally suggested the valence state of Co (*vide infra*).

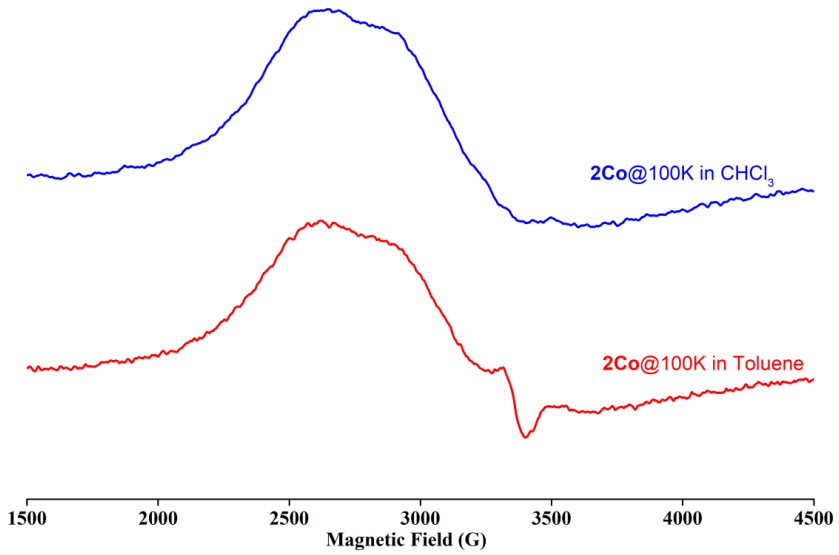

Fig. S13 X-band EPR Spectra of **2Co** in $CHCl_3$ and toluene at 100 K. EPR parameters: microwave frequency 9.395 GHz, incident microwave power 0.976 mW, modulation frequency 100 kHz.

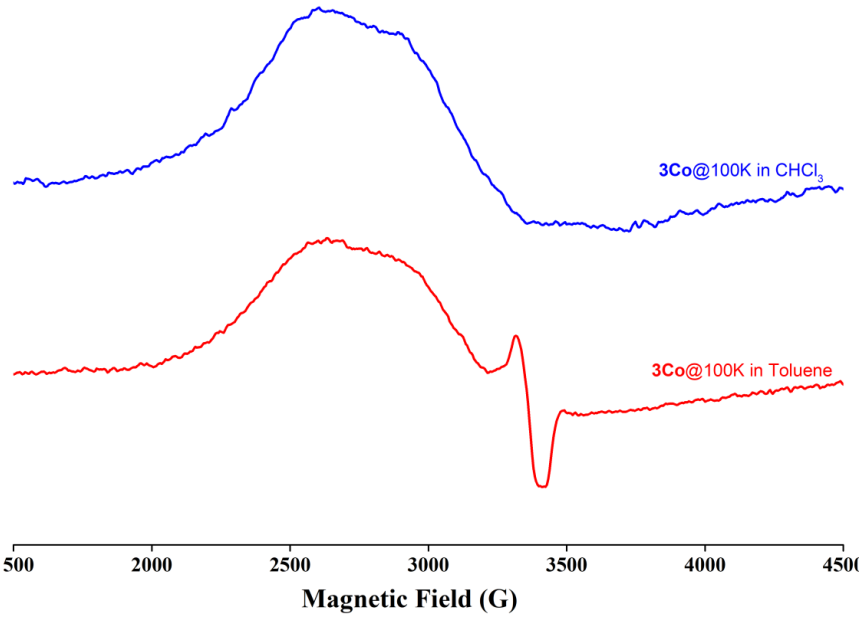

Fig. S14 X-band EPR Spectra of **3Co** in $CHCl_3$ and toluene at 100 K. EPR parameters: microwave frequency 9.395 GHz, incident microwave power 0.976 mW, modulation frequency 100 kHz.

Mass Analysis: The synthesized porphyrins embedded onto the MWCNT for catalysis (**1Co**, **2Co** and **3Co**) and its parent molecules are characterized by MALDI-TOF mass spectrometry in positive ion mode and presented in Figs. S15-S20. In all the cases, the observed mass values are in good agreement with the calculated mass values.

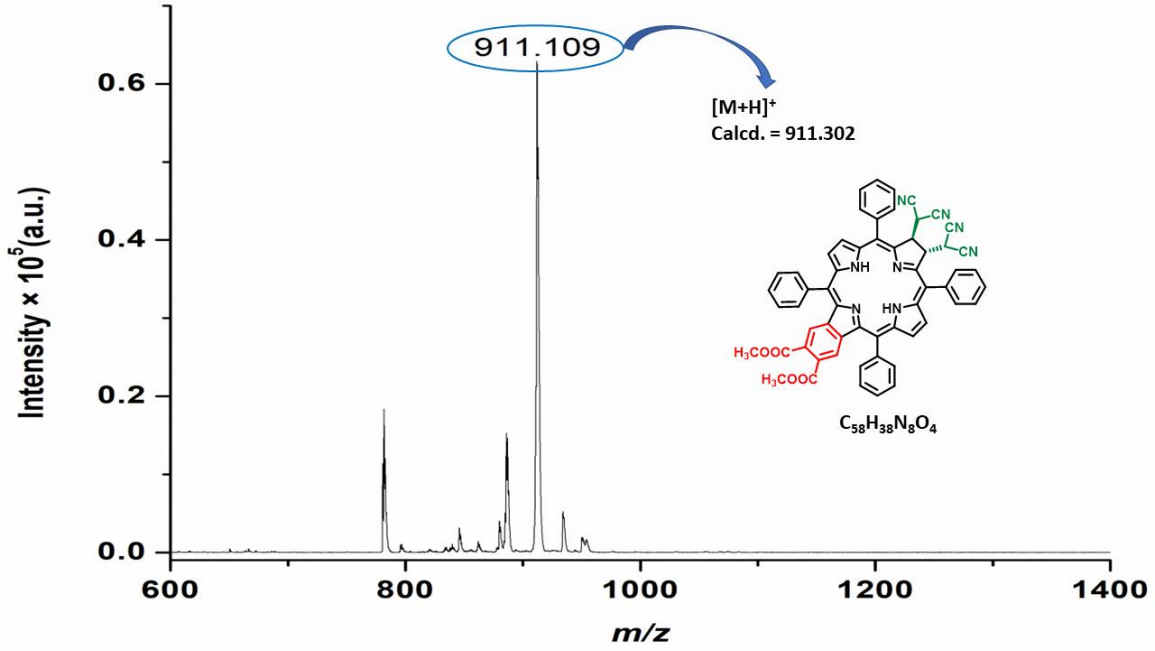

Fig. S15 MALDI-TOF mass spectrum of H_2TPCMB(MN)$_2$ in positive ion mode at 298 K.

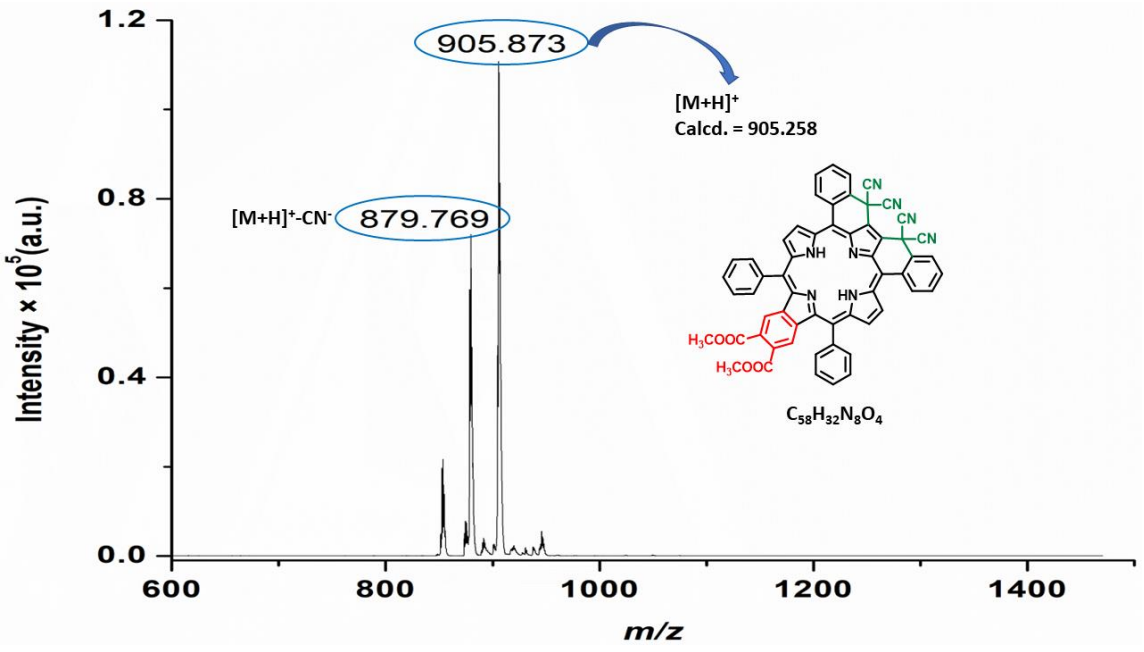

Fig. S16 MALDI-TOF mass spectrum of H_2TFPMB(MN)$_2$ in positive ion mode at 298 K.

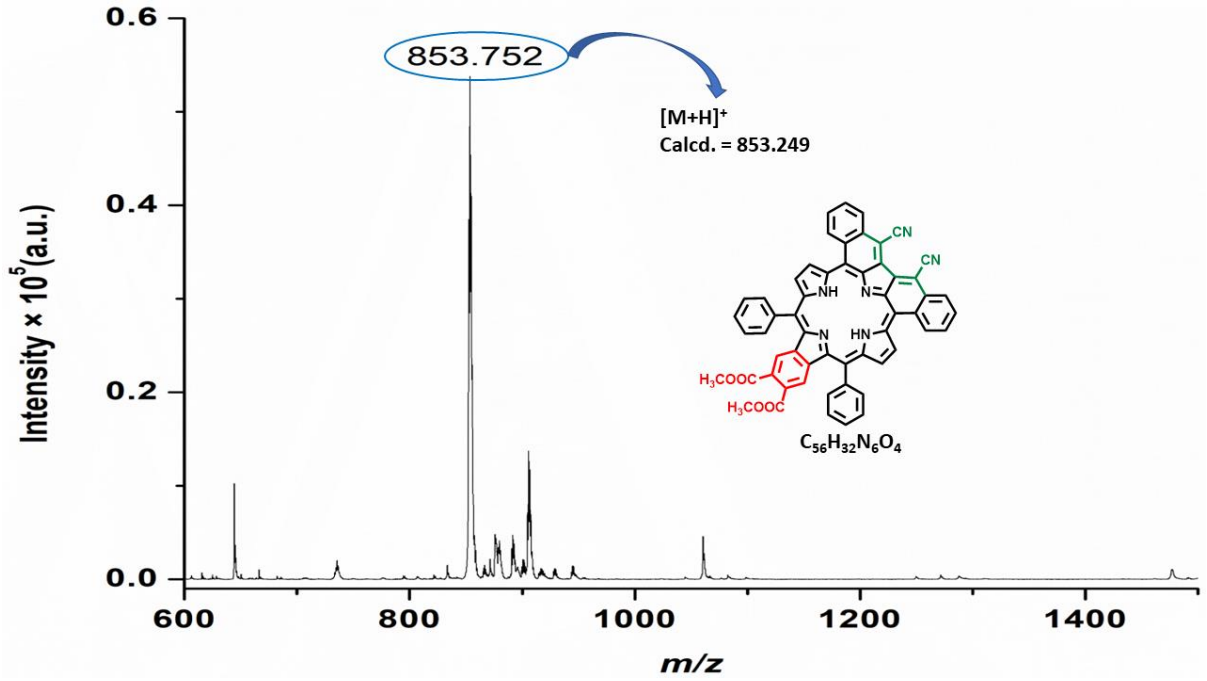

Fig. S17 MALDI-TOF mass spectrum of H_2TFPMB(VCN)$_2$ in positive ion mode at 298 K.

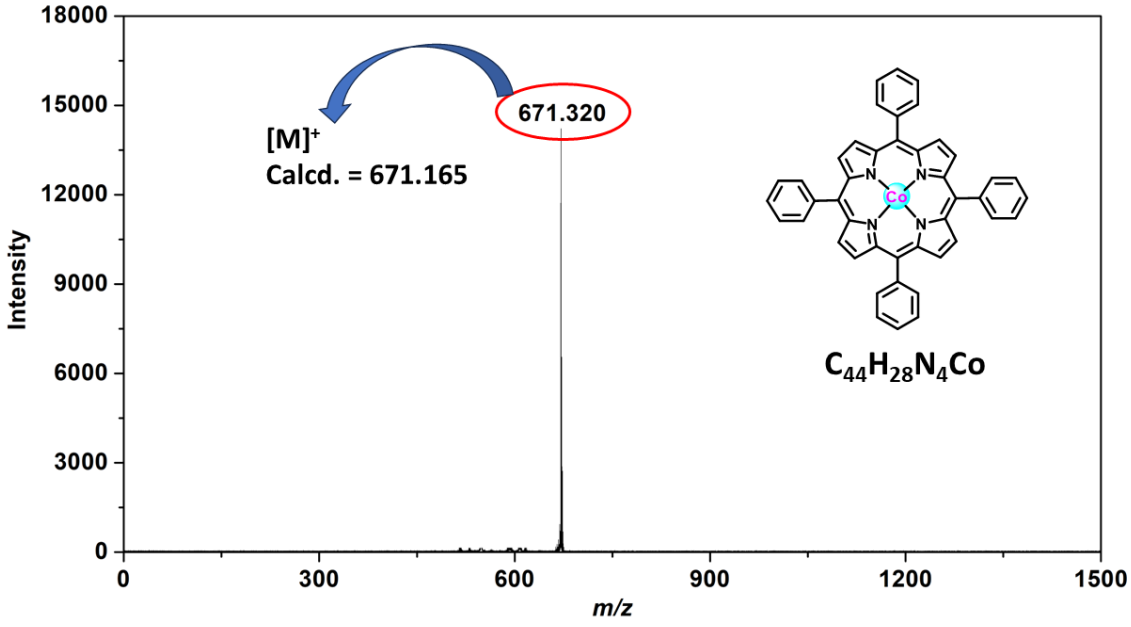

Fig. S18 MALDI-TOF mass spectrum of CoTPP (**1Co**) in positive ion mode at 298 K.

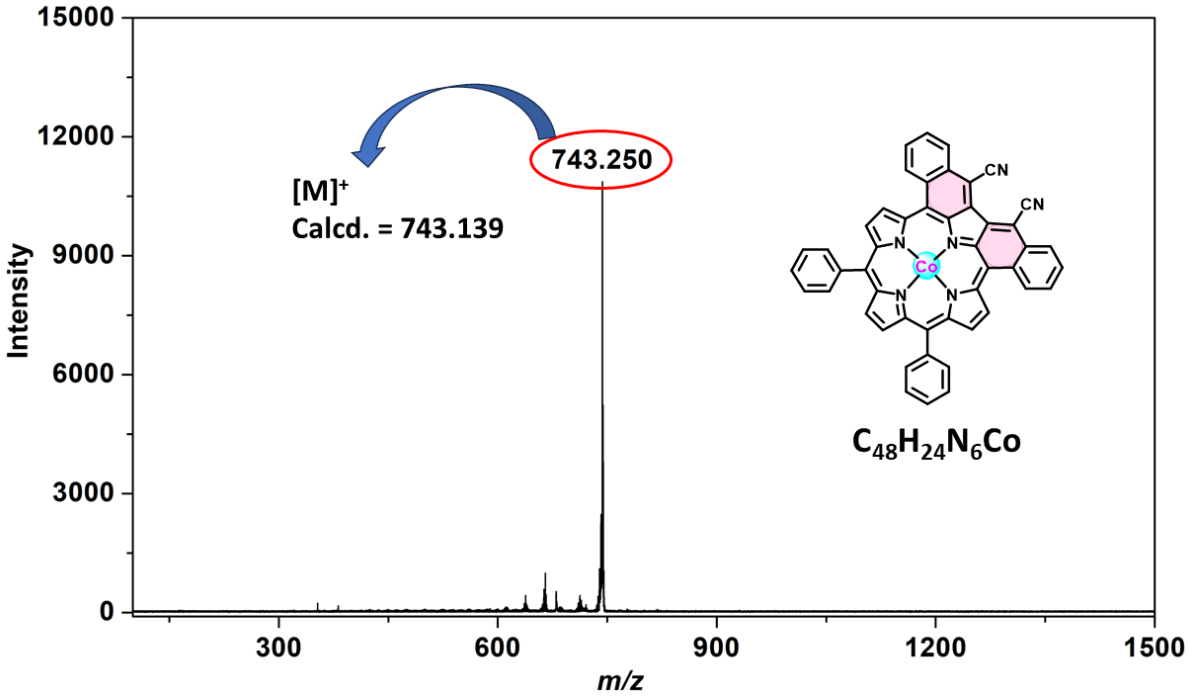

Fig. S19 MALDI-TOF mass spectrum of CoDFP(VCN)2 (**2Co**) in positive ion mode at 298 K.

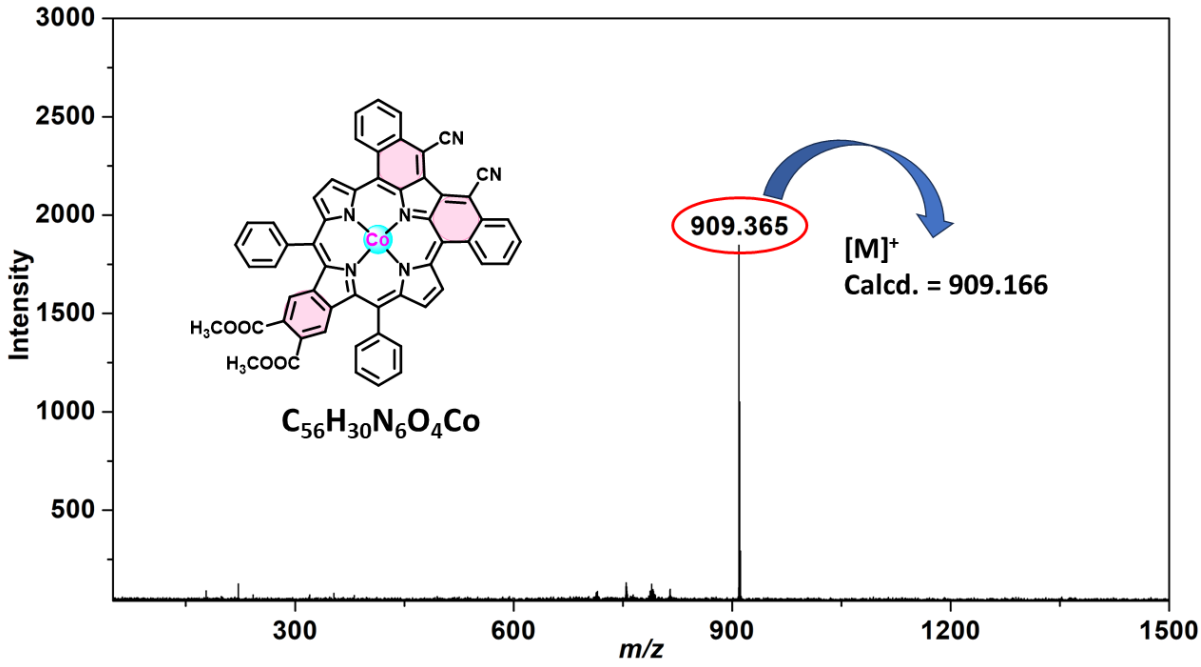

Fig. S20 MALDI-TOF mass spectrum of CoTFPMB(VCN)2 (**3Co**) in positive ion mode at 298 K.

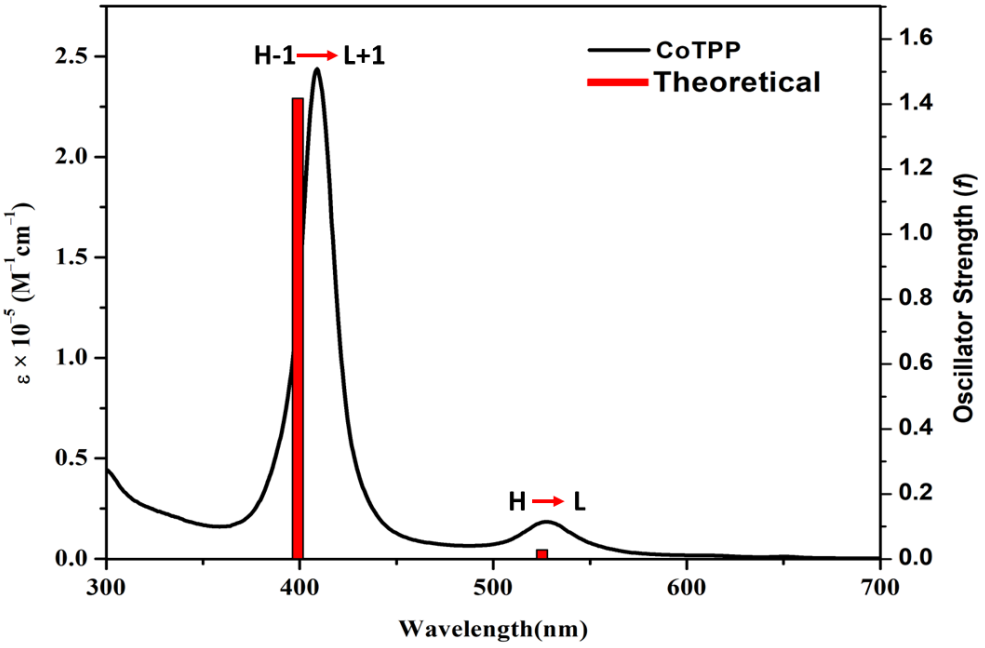

Fig. S21 Comparative (theoretical and experimental) absorption spectra of CoTPP (**1Co**).

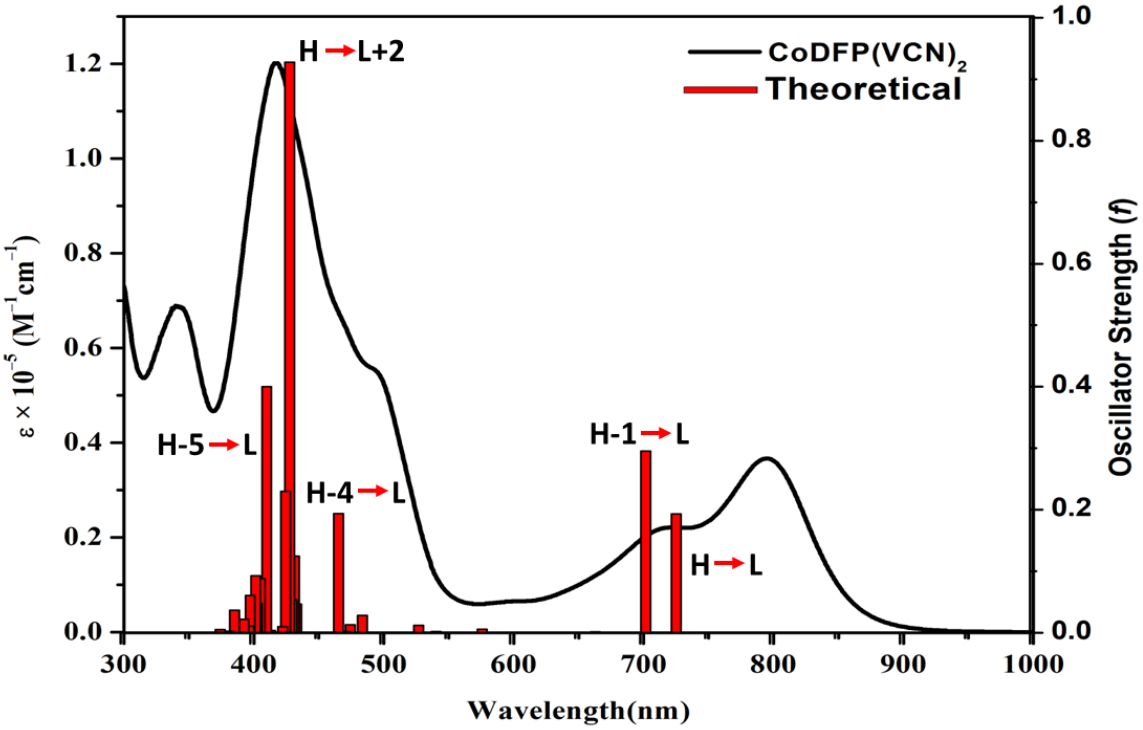

Fig. S22 Comparative (theoretical and experimental) absorption spectra of CoDFP(VCN)$_2$ (**2Co**).

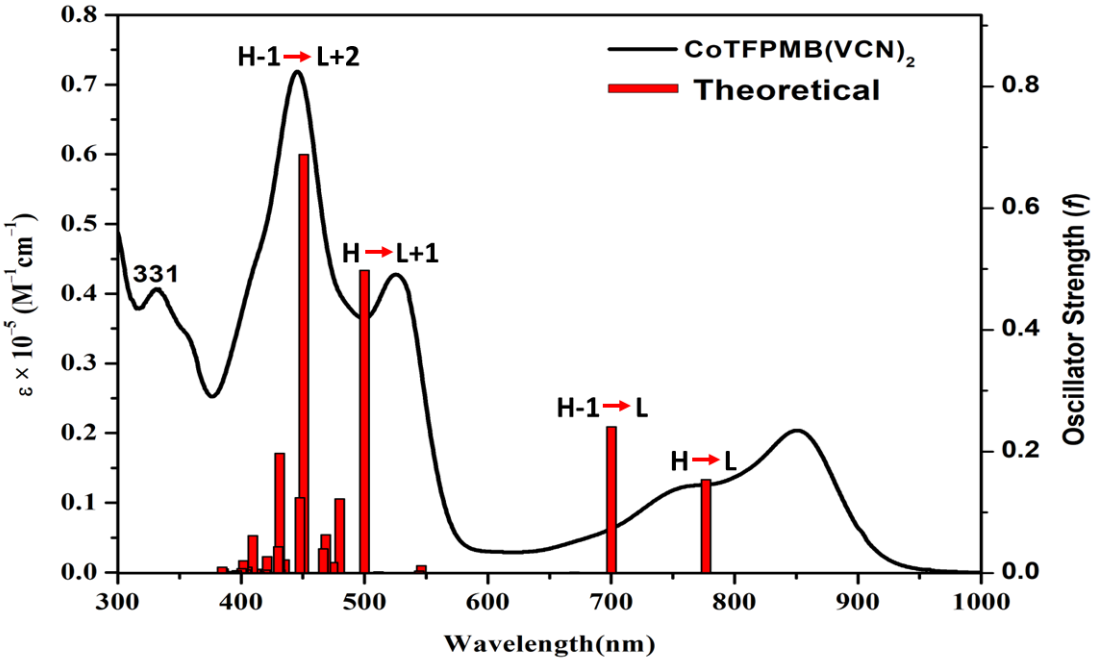

Fig. S23 Comparative (theoretical and experimental) absorption spectra of CoTFPMB(VCN)$_2$ (**3Co**).

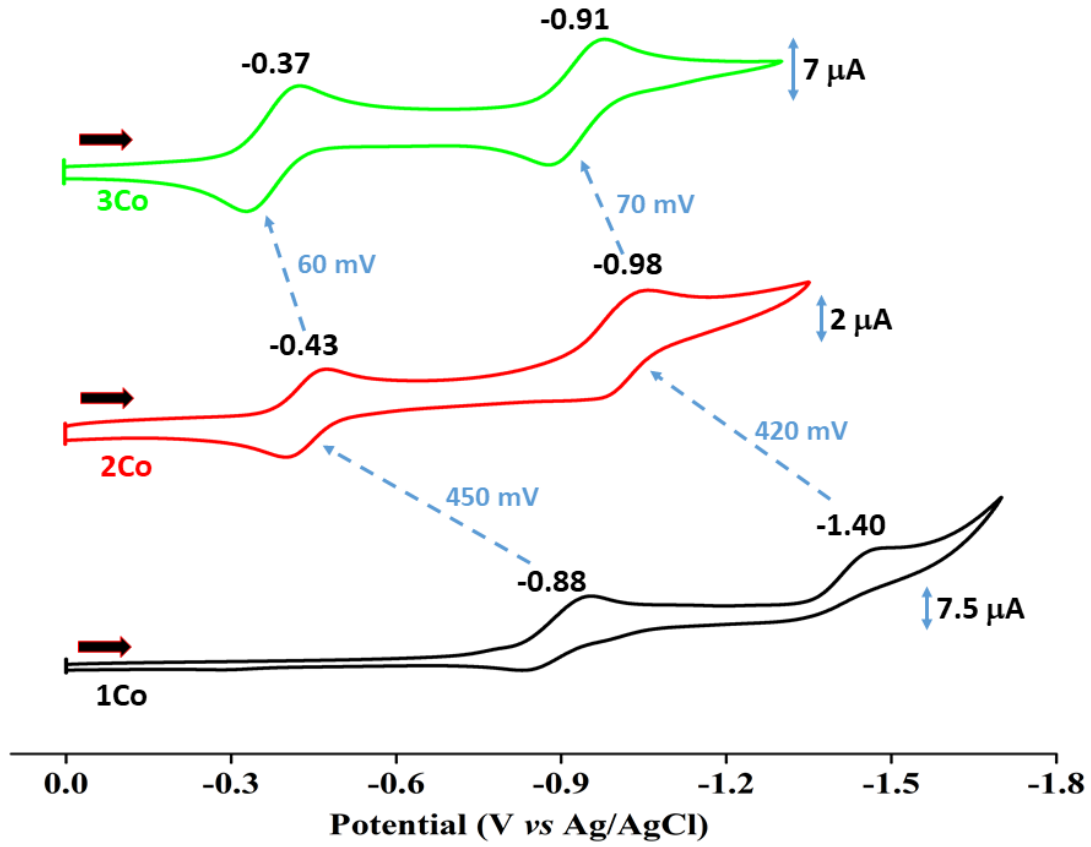

Fig. S24 Cyclic Voltammograms comparing the reductions of **1Co**, **2Co** and **3Co** in CH_2Cl_2 at 298 K. Scan rate = 0.1 Vs^{-1}.

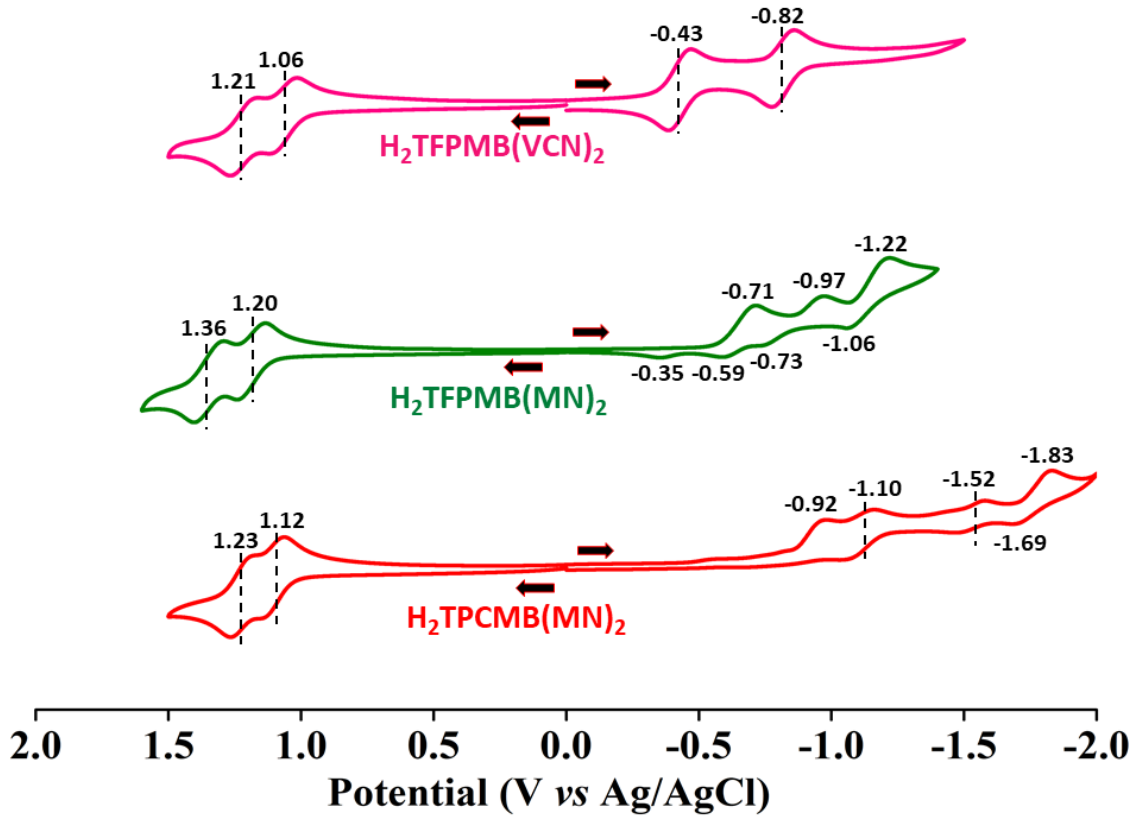

Fig. S25 Cyclic voltammograms of $H_2TPCMB(MN)_2$, $H_2TFPMB(MN)_2$, and $H2TFPMB(VCN)_2$ in CH_2Cl_2 at 298 K using $TBAPF_6$ as a supporting electrolyte. Scan rate = 100 mV/s.

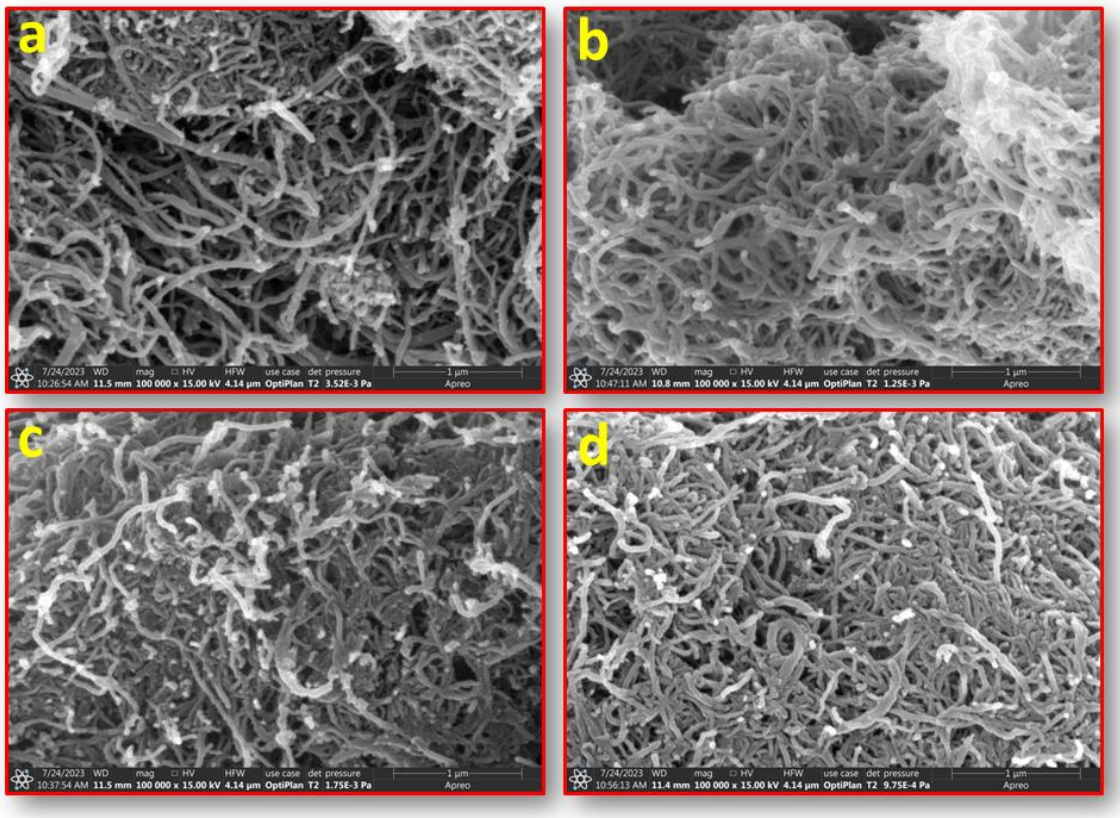

Fig. S26 SEM images of (a) bare MWCNT, (b) **1Co**@MWCNT, (c) **2Co**@MWCNT, and (d) **3Co**@MWCNT.

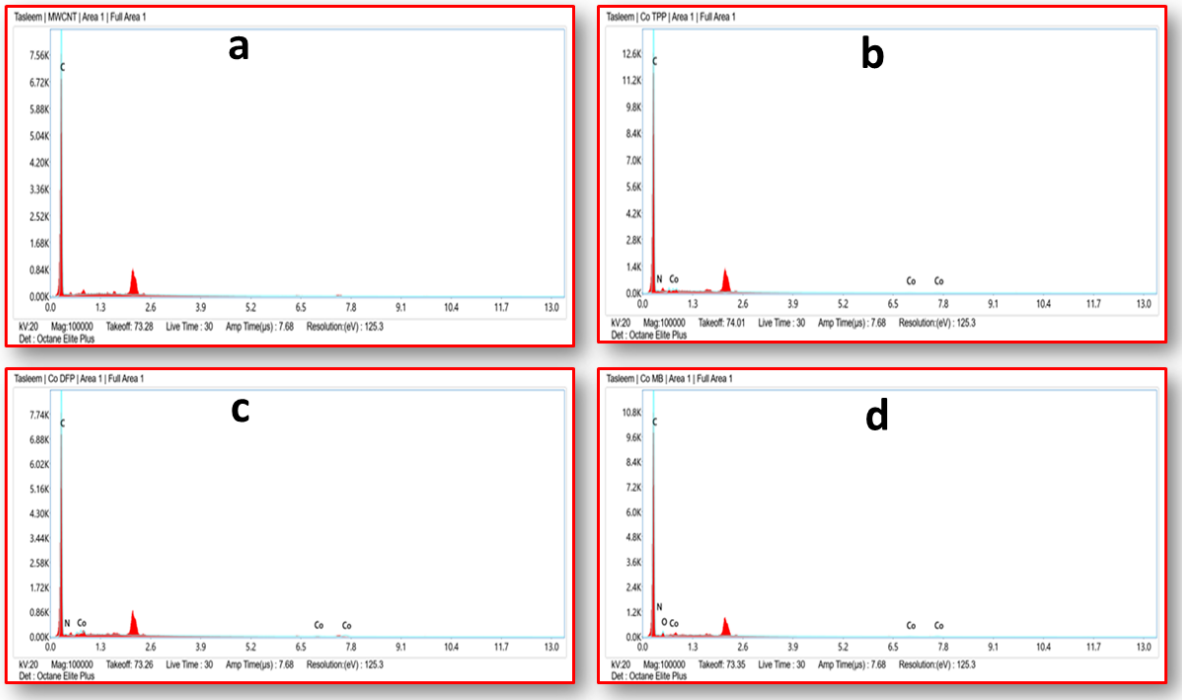

Fig. S27 EDAX patterns of (a) bare MWCNT, (b) **1Co**@MWCNT, (c) **2Co**@MWCNT, and (d) **3Co**@MWCNT.

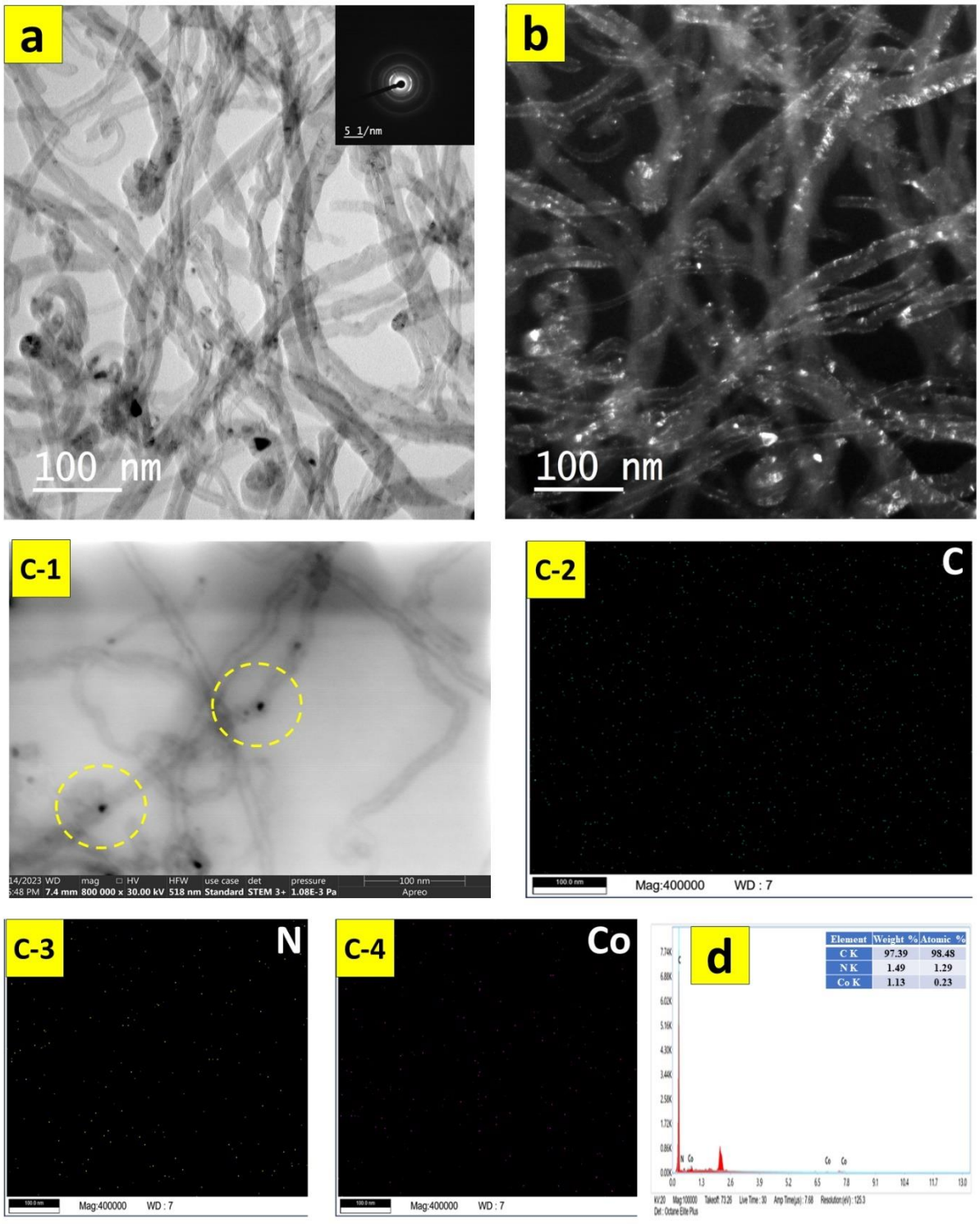

Fig. S28 HR-TEM Bright-Field (a) and Dark-Field (b) images, HAADF-STEM mapping images (C-1 to C-4) and the EDAX spectrum (d) of **2Co**@MWCNT. Inset of (a) represents the SAED pattern. The circles in the image (C-1) indicate the presence of **2Co**.

Powder XRD: The PXRD of the composites are shown in Fig. S29. The XRD pattern of MWCNT shows two peaks at 25.7° and 43.5° (2θ) corresponding to (002) and (100) planes of hexagonal graphitic structure.[S2,S7] In the nanocomposites (**1Co**@MWCNT, **2Co**@MWCNT and **3Co**@MWCNT), the peaks at 2θ = 43.5° are significantly compressed due to the strong porphyrin-MWCNT electronic interaction that may result in some distortion in the structure indicating the successful adsorption of **1Co**, **2Co,** and **3Co** on the MWCNT surface.[S8,S9]

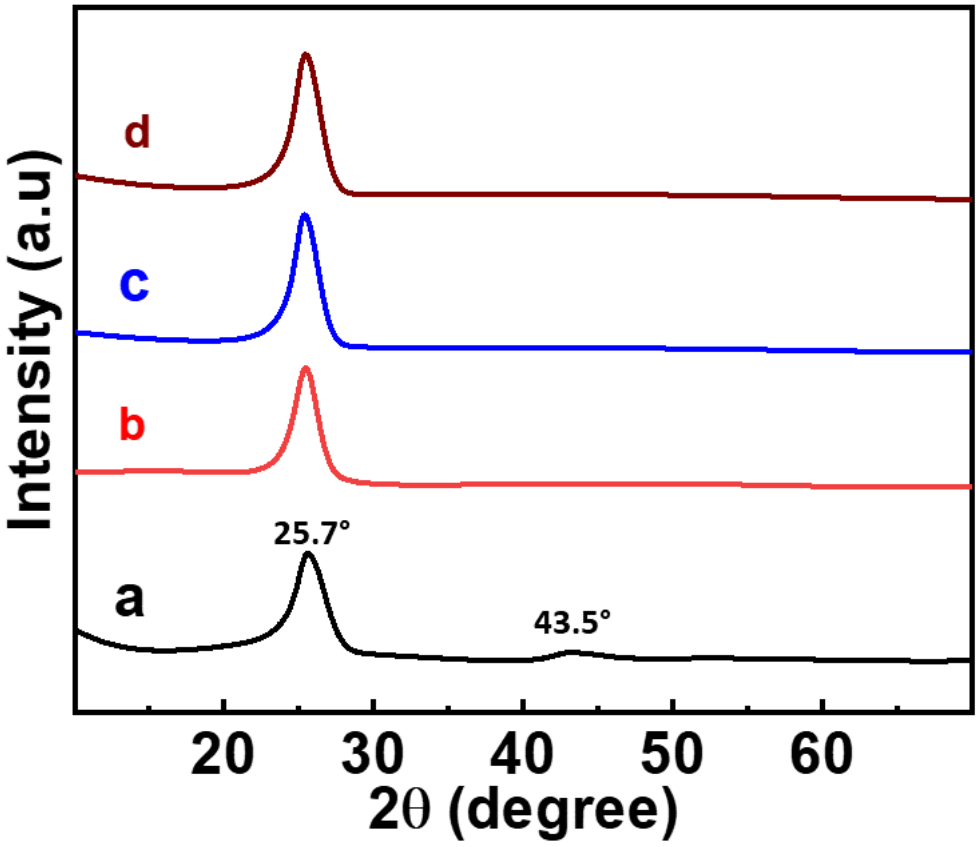

Fig. S29 Powder XRD patterns of (a) MWCNT, (b) **1Co**@MWCNT, (c) **2Co**@MWCNT, and (d) **3Co**@MWCNT.

Raman Spectroscopy: The successful formation of the nanocomposites was further evidenced by Raman spectroscopy. The two principal spectral bands namely, D and G bands were appeared in the expected Raman frequency region for all the investigated nanocomposites along with bare MWCNT (Fig. S30 and Table S5). In general, when the nanomaterials are functionalized with electron acceptor moieties, the Raman frequency shifts to the higher region whereas electron donor moieties shift to the lower region.[S10] In the present case, all the nanocomposites exhibit the shifts to the higher frequency for both D and G bands than bare MWCNT suggesting the electron deficient nature of the porphyrin core due to extended π-conjugation. The intensity ratio of the D band to the G band (I_D/I_G) implies the extent of surface modification of the MWCNT (Table S5). The decrease in the I_D/I_G of the nanocomposites relative to bare MWCNT suggests the successful surface modification of the MWCNT.[S11,S12] Moreover, the weak signals at low wavelength region were observed due to the presence of the porphyrins in the nanocomposites, which further support the successful immobilization of porphyrins onto the MWCNTs.[S8]

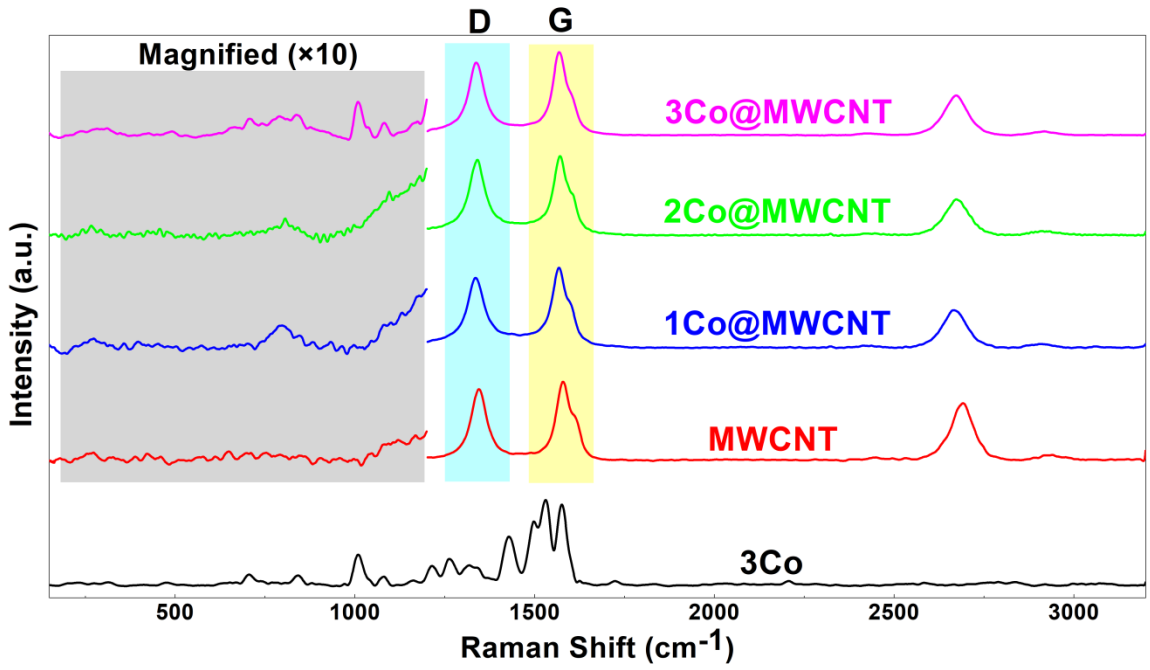

Fig. S30 Raman spectra of **3Co**, bare MWCNT, **1Co**@MWCNT, **2Co**@MWCNT, and **3Co**@MWCNT.

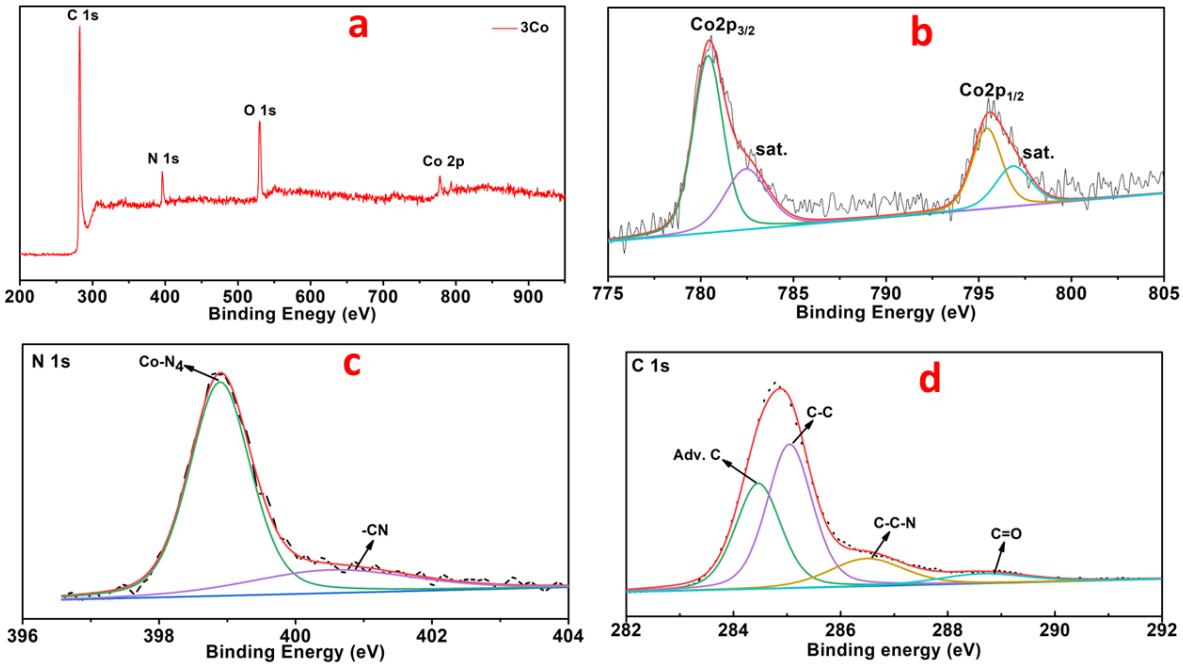

Fig. S31 (a) XPS survey scan of **3Co**@MWCNT and a representative XPS narrow scans for (b) Cobalt (Co 2p), (c) Nitrogen (N1s) and (d) Carbon (C1s) present in **3Co**@MWCNT.

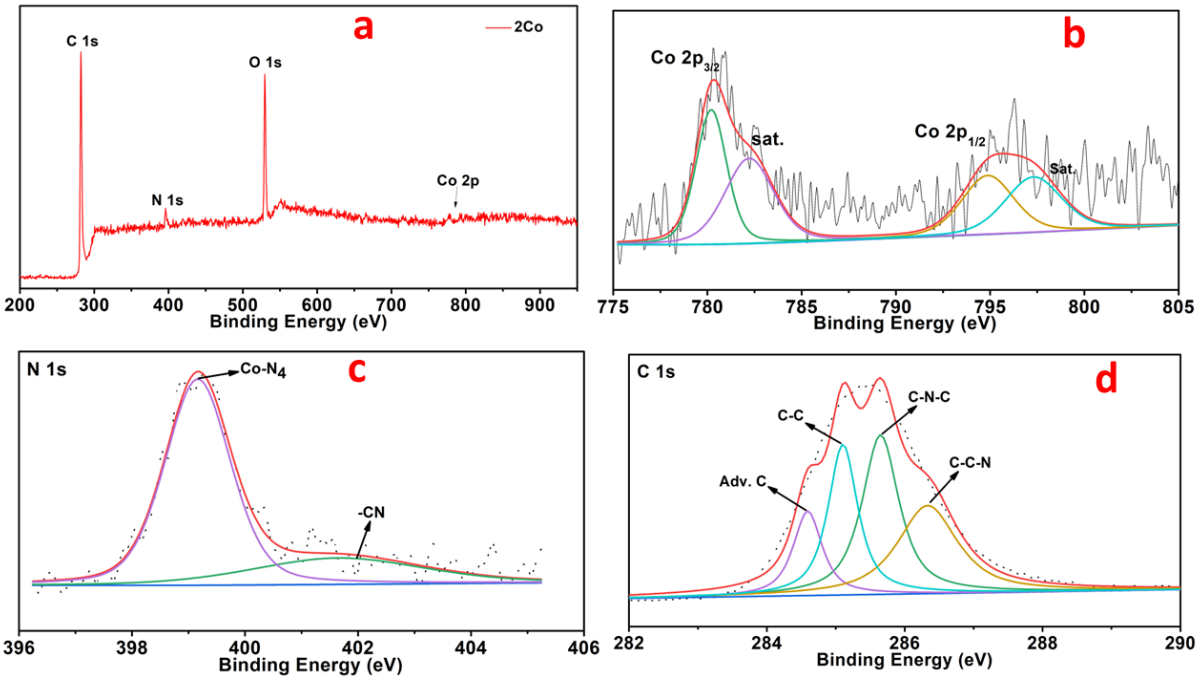

Fig. S32 (a) XPS survey scan of **2Co**@MWCNT and a representative XPS narrow scans for (b) Cobalt (Co 2p), (c) Nitrogen (N1s) and (d) Carbon (C1s) present in **2Co**@MWCNT.

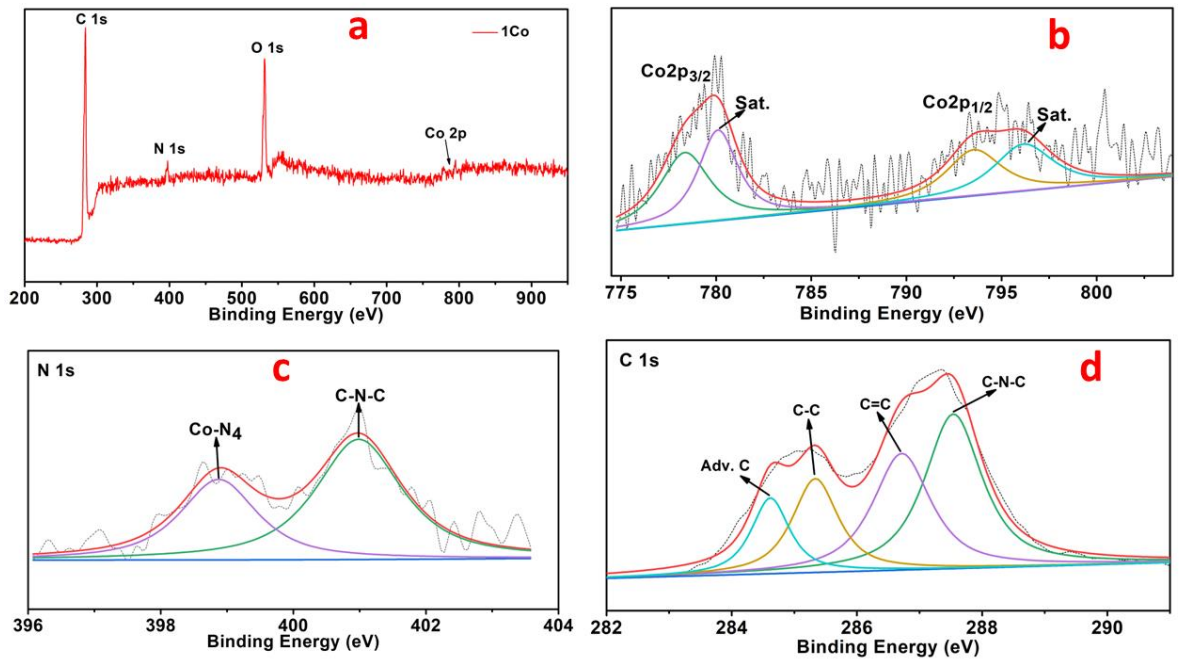

Fig. S33 (a) XPS survey scan of **1Co**@MWCNT and a representative XPS narrow scans for (b) Cobalt (Co2p), (c) Nitrogen (N1s), and (d) Carbon (C1s) present in **1Co**@MWCNT.

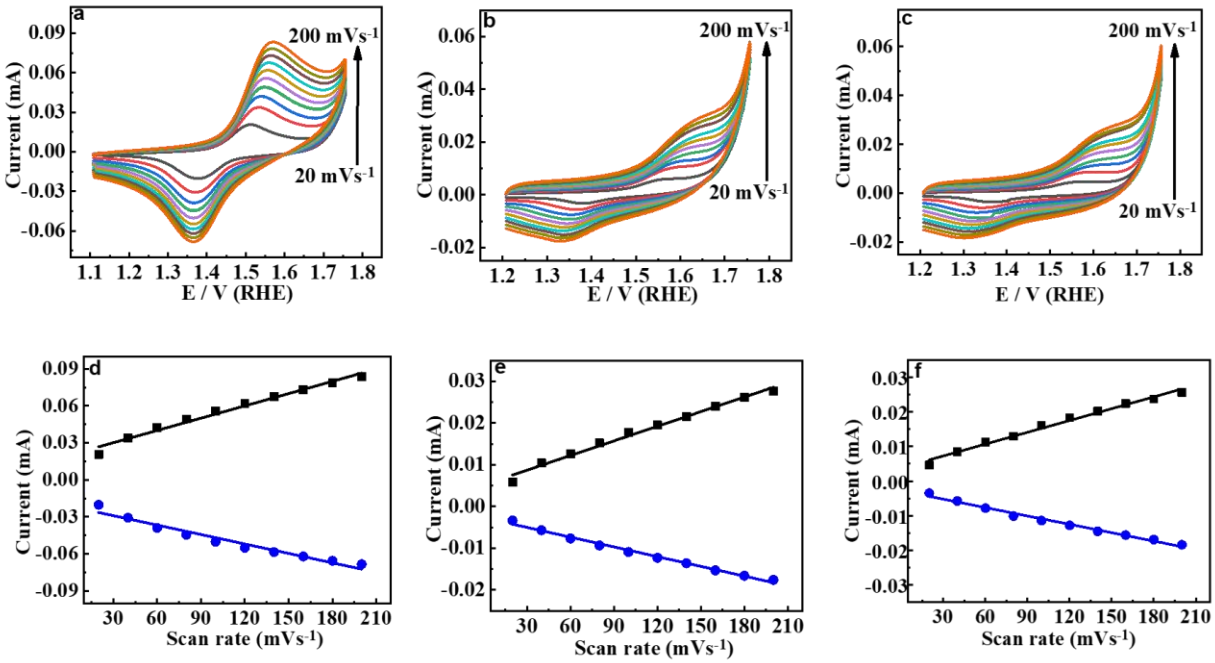

Fig. S34 CV response of **1Co** (a), **2Co** (b), and **3Co** (c) coated on GC electrodes at different scan rates in 1.0 M KOH and the corresponding current *vs.* scan rate plots (d-f, respectively).

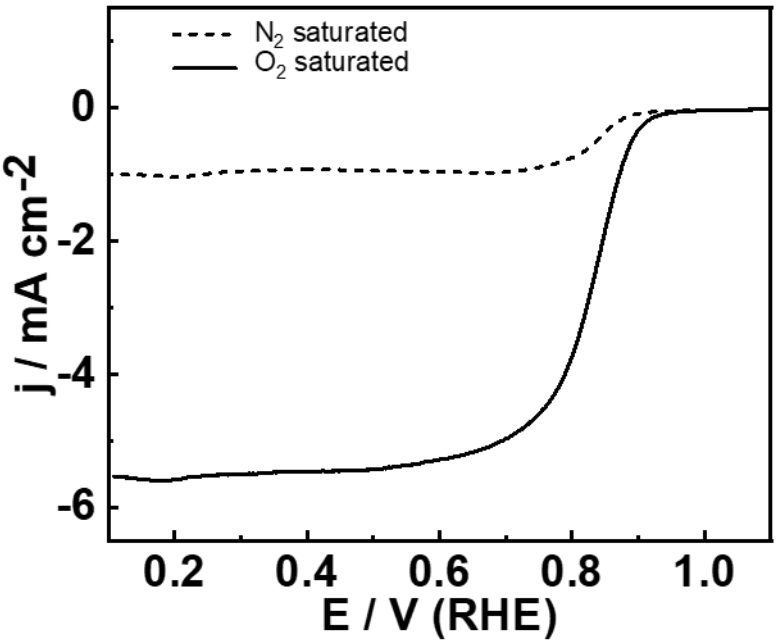

Fig. S35: LSV response Pt/C in 0.1 M KOH.

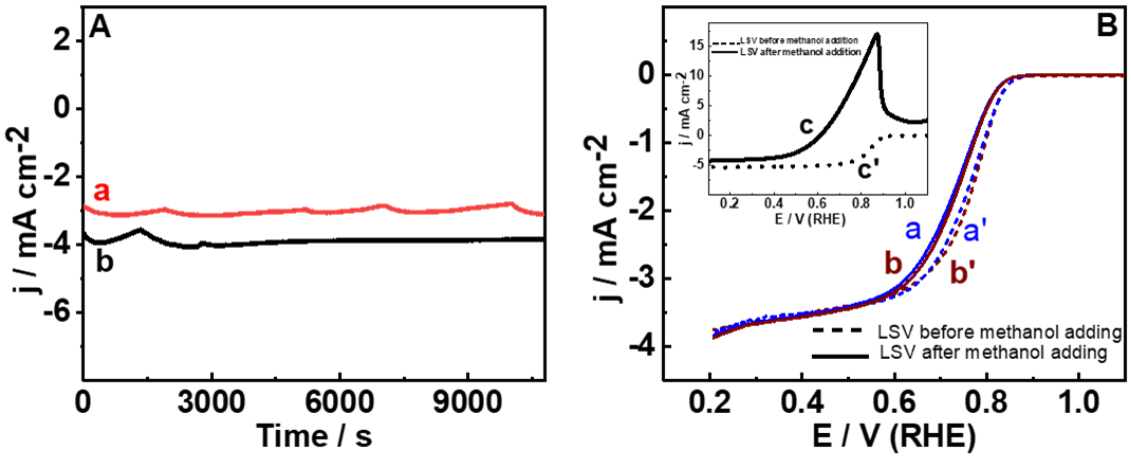

Fig. S36 (A) Amperometry responses of **2Co**@MWCNT (a) and **3Co**@MWCNT (b) for 10800 s at an applied potential of 0.5 V (*vs.* RHE) and a rotation rate of 1600 rpm. (B) LSV responses of **2Co**@MWCNT (a, a') and **3Co**@MWCNT (b, b') before (a', b') and after (a, b) the addition of 3.0 M methanol. Inset of B shows the LSV responses of Pt/C before (c') and after (c) the addition of 3.0 M methanol.

Post-Catalysis Powder XRD: The powder XRD patterns of bare indium doped tin oxide (ITO) and **3Co**@MWCNT coated ITO are shown in Fig. S37. The pre- and post-catalysis (after 2 h of amperometry) XRD patterns of **3Co**@MWCNT coated ITO shows almost no change indicating the absence of agglomeration and no changes in the crystallinity of the material during the ORR which suggests the high durability of the catalyst. The peak at 26.1˚ implies the presence of the catalyst, **3Co**@MWCNT on the ITO glass.

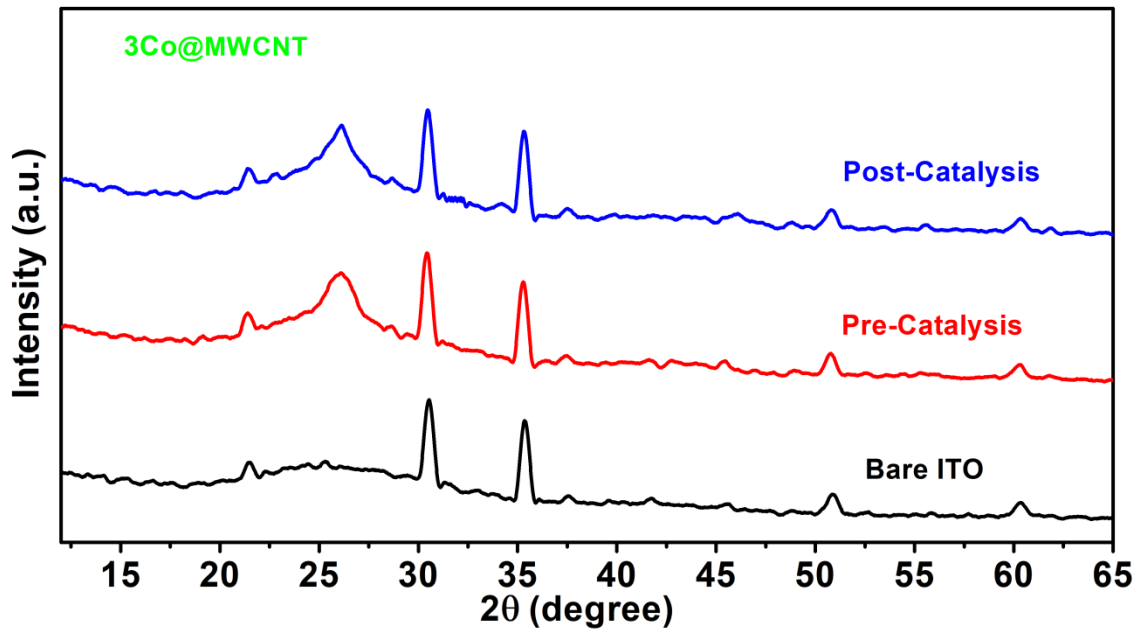

Fig. S37 Powder XRD patterns of bare ITO (black line), **3Co**@MWCNT coated ITO before catalysis (red line) and after catalysis (blue line).

Post-Catalysis Raman Spectroscopy: The Raman spectra of bare indium doped tin oxide (ITO) and **3Co**@MWCNT coated ITO are shown in Fig. S38. The pre- and post-catalysis (after 2 h of amperometry) Raman spectral features of **3Co**@MWCNT coated ITO shows similar pattern indicating no change in the crystallinity during ORR which suggests the high durability of the catalyst. The weak peak at the lower wavelength indicates the presence of **3Co** in the catalyst.[S8]

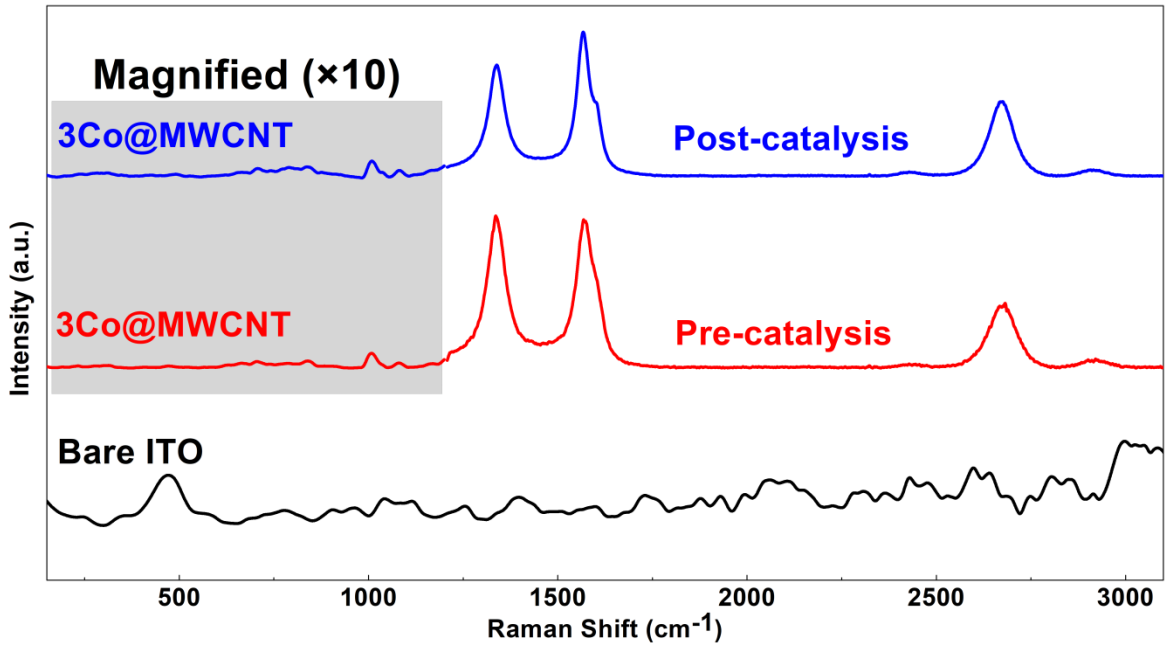

Fig. S38: Raman spectra of bare ITO (black line), **3Co**@MWCNT coated ITO before catalysis (red line), and after catalysis (blue line).

Post-Catalysis SEM: The SEM images and corresponding EDAX patterns of **3Co**@MWCNT coated on ITO plate are shown in Fig. S39. The pre- and post-catalysis (after 2 h of amperometry) SEM images of **3Co**@MWCNT coated on ITO plate shows almost similar surface of the material.

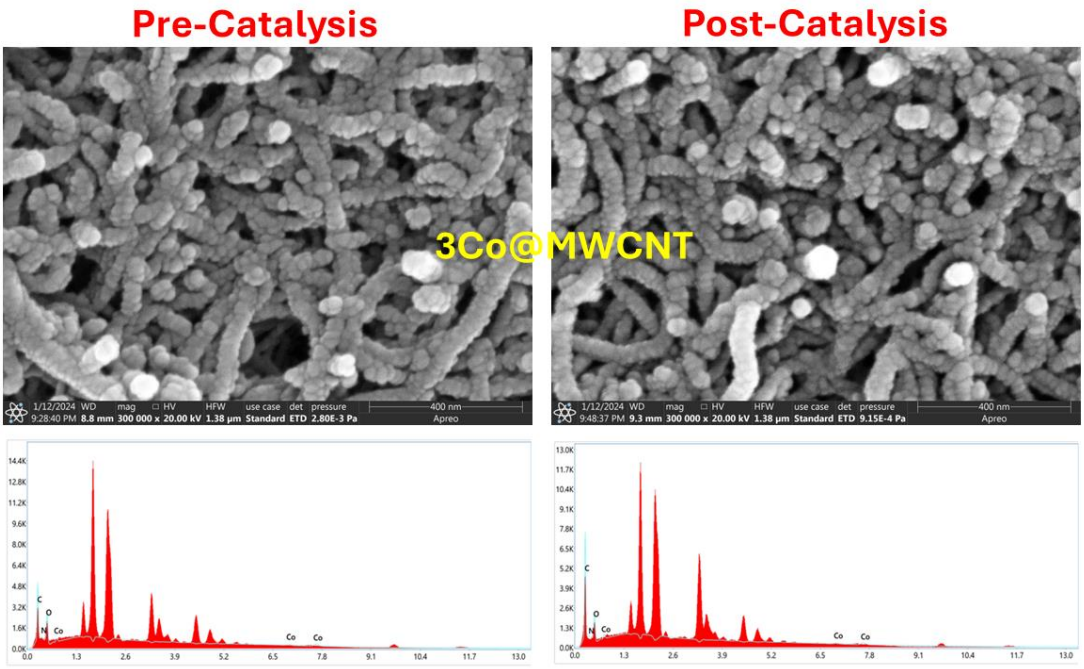

Fig. S39: SEM images of **3Co**@MWCNT coated on ITO and their corresponding EDAX patterns before and after catalysis.

Post-Catalysis AFM: The pre- and post-catalysis (after 2 h of amperometry) AFM images of **3Co**@MWCNT coated on ITO plate are shown in Fig. S40. The pre- and post-catalysis AFM images show negligible changes on the surface morphology of the material.

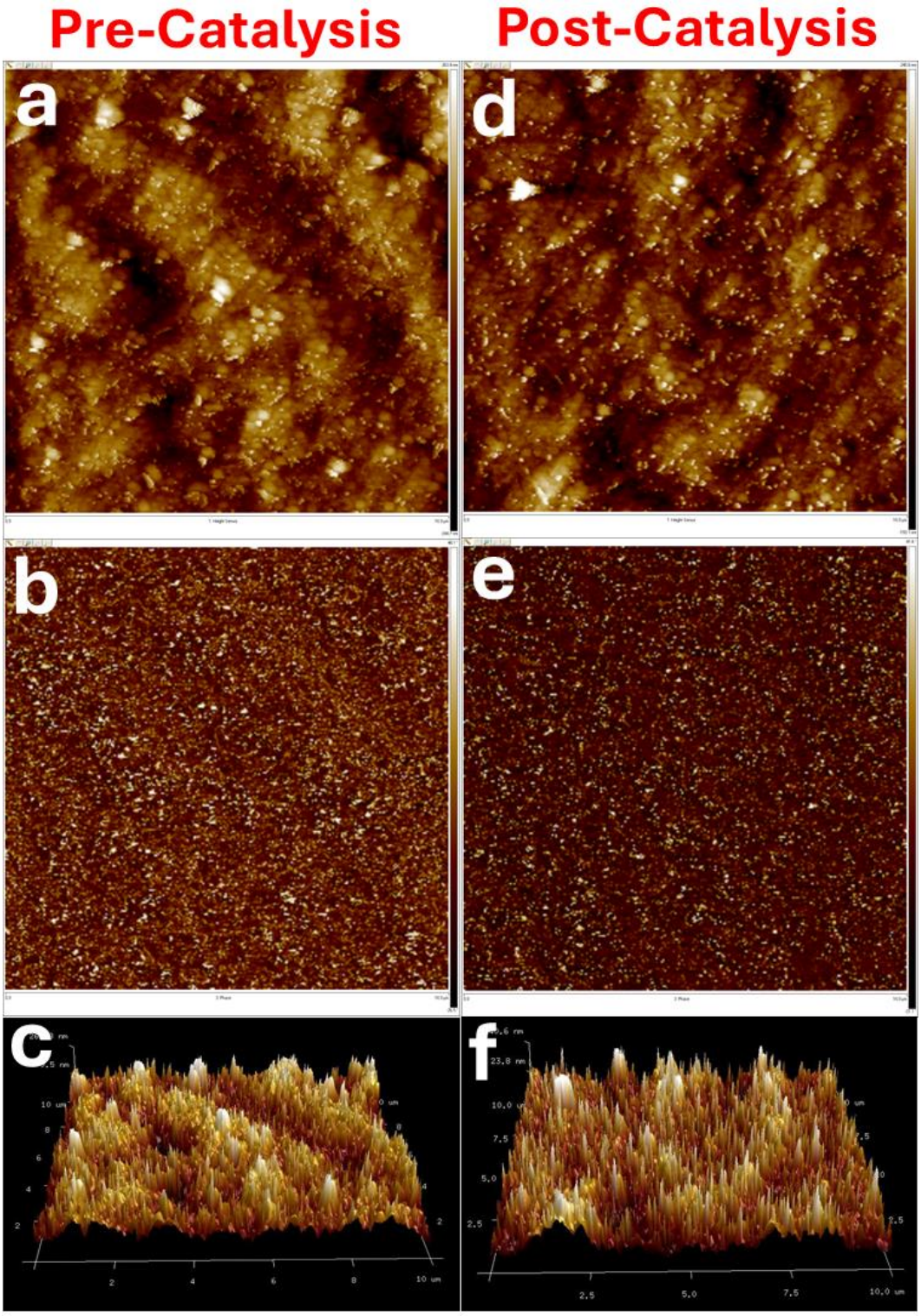

Fig. S40: Contact mode AFM images of **3Co**@MWCNT coated on ITO plate: Pre-catalysis 2D topography frame (a), lateral force frame (b), and 3D topology frame (c) and post-catalysis 2D topography frame (d) lateral force frame (e), and 3D topology frame (f).

Table S1 UV-Vis Absorption Spectral Data of Synthesized Porphyrins[a].

Porphyrin	**λ_{abs}, nm**
CoTPP (**1Co**)	409 (244), 528 (183)
CoDFP(VCN)$_2$ (**1Co**)	340 (69), 418 (120), 496 (55), 723 (22), 796 (37)
H_2TPCMB(MN)$_2$	407(sh) (200), 428 (891), 516 (52), 558 (12), 610 (19), 666 (92)
H_2TFPMB(MN)$_2$	486 (619), 582 (39), 631 (13), 663 (15), 730 (39)
H_2TFPMB(VCN)$_2$	344 (36), 363 (36), 434 (99), 480 (40), 518 (49), 754 (14), 840 (26)
CoTFPMB(VCN)$_2$ (**3Co**)	331 (41), 445 (72), 526 (43), 763 (12), 851 (20)

[a]Values in parentheses refer to $\varepsilon \times 10^{-3}$Lmol^{-1}cm^{-1}, sh = shoulder.

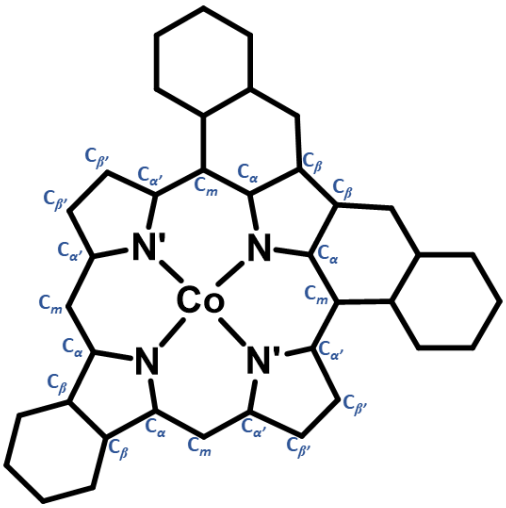

Table S2 Crystallographic data of **Co(Cl)TFPMB(VCN)$_2$•(CH$_3$OH).**

	Co(Cl)TFPMB(VCN)$_2$•(CH$_3$OH)
Empirical Formula	$C_{57}H_{34}ClCoN_6O_5$
Formula Wt.	977.28 g/mol
Crystal System	Triclinic
Space Group	P -1
a (Å)	10.5787(5)
b (Å)	13.3611(6)
c (Å)	18.6693(8)
α (°)	73.222(2)
β (°)	89.394(2)
γ (°)	84.620(2)
Volume (Å^3)	2514.9(2)
Z	2
D_{calcd} (g/cm^3)	1.291
Wavelength (Å)	0.71073
T (°C)	104 K
No. of total reflns.	125502

No. of Indepnt. reflns.	9076
R	0.0777
GOOF	1.054
CCDC No.	2290977
	Bond Length (Å)
M-N	1.932(5)
M-N'	1.933(3)
N-C_{α}	1.378(5)
N'-$C_{\alpha'}$	1.373(5)
C_{α}-C_{β}	**1.443(6)**
$C_{\alpha'}$-$C_{\beta'}$	**1.435(6)**
C_{β}-C_{β}	1.426(6)
$C_{\beta'}$-$C_{\beta'}$	1.358(6)
C_{α}-C_{m}	1.395(6)
$C_{\alpha'}$-C_{m}	1.407(5)
ΔC_{β} (Å)	**0.283**
Δ24 (Å)	**0.367**
Δ38 (Å)	**0.672**
ΔM	0.021
	Bond Angles (°)
M-N-C_{α}	126.33(2)
M-N'-$C_{\alpha'}$	126.54(3)
N-M-N	179.36(14)
N'-M-N'	178.29(14)
N-C_{α}-C_{m}	124.65(3)
N'-$C_{\alpha'}$-C_{m}	124.10(4)
N-C_{α}-C_{β}	110.37(3)
N'-$C_{\alpha'}$-$C_{\beta'}$	109.66(4)
C_{β}-C_{α}-C_{m}	124.60(4)
$C_{\beta'}$-$C_{\alpha'}$-C_{m}	125.65(4)
C_{α}-C_{m}-$C_{\alpha'}$	121.33(4)
C_{α}-C_{β}-C_{β}	105.90(4)
$C_{\alpha'}$-$C_{\beta'}$-$C_{\beta'}$	107.02(4)
C_{α}-N-C_{α}	107.19(3)
$C_{\alpha'}$-N-$C_{\alpha'}$	106.42(2)

ΔC_{β} refers to the mean plane displacement of the β-pyrrolic carbons.
Δ24 refers to the mean plane deviation of the 24-core atom.
Δ38 refers to the mean plane deviation of the 38-core atom.

Table S3 Deviations of core atoms from the mean plane using DFT calculation.

	CoTPP	**CoDFP(VCN)$_2$**
ΔC_{β} (Å)	0.217	0.553
Δ24 (Å)	0.100	0.308

Table S4 Calculated electronic excitation energies, major orbital contribution, theoretical and experimental absorption maxima, and oscillatory strength of investigated porphyrins.

Porphyrin	Excited state energy (eV)	Contribution	Coefficient	λ (nm)	Oscillatory strength (f)	Experimental λ_{max} (nm) in CH_2Cl_2
1Co	3.108	HOMO-1 → LUMO+1	53	399	1.57	409
	2.063	HOMO → LUMO				
2Co	2.882	HOMO → LUMO+2	41	430	0.928	418
	3.005	HOMO-5 → LUMO				
	2.650	HOMO-4 → LUMO				
	1.760	HOMO-1 → LUMO				
	1.703	HOMO → LUMO				
3Co	2.751	HOMO-1 → LUMO+2	35	451	0.856	445
	2.486	HOMO → LUMO+1	55	500	0.614	526
	1.771	HOMO-1 → LUMO				
	1.596	HOMO → LUMO				

Table S5 Raman spectral data of MWCNT and synthesized nanocomposites.

Samples	Frequency (cm^{-1})		I_D/I_G
	D band	G band	
MWCNT	1335	1565	1.012
1Co@MWCNT	1337	1567	0.804
2Co@MWCNT	1343	1574	0.819
3Co@MWCNT	1340	1570	0.860

Table S6 Comparison of the ORR efficiency of **2Co**@MWCNT and **3Co**@MWCNT with other catalysts in terms of E_{onset} and $E_{1/2}$ values.

Material	E_{onset} (V *vs.* RHE)	$E_{1/2}$ (V *vs.* RHE)	References
CoTMPP@MCN[A]	0.84	0.62	S13
1Co@MWCNT	0.81	0.63	This work
2Co@MWCNT	0.88	0.79	This work
3Co@MWCNT	0.90	0.80	This work
CoCOF-Py-Rgo[B]	0.83	0.765	S14
CoPor/C[C]	0.80	0.70	S15
TPABT-CoPor/C[D]	0.72	0.58	S15
BTDCoPor/C[E]	0.77	0.47	S15
F-CoPor/C[F]	0.62		S16
AC-CoPor/C[G]	0.72		S16
CN-CoPor/C[H]	0.76		S16

[A] Cobalt tetramethoxyphenylporphyrin integrated on mesoporous carbon nitride; [B] Cobalt porphyrin-based covalent organic framework on functionalized reduced graphene oxide; [C] cobalt porphyrins substituted with methyl phenyl groups integrated on carbon black; [D] cobalt porphyrins substituted with 2,1,3-benzothiadiazole groups integrated on carbon black; [E] cobalt porphyrins substituted with 2,1,3-benzothiadiazole triphenylamine groups integrated on carbon black; [F] cobalt *meso*-tetraaryl porphyrins with fluorine; [G] cobalt *meso*-tetraaryl porphyrins with acetic acid; [H] cobalt *meso*-tetraaryl porphyrins with cyanoacetic acid.

References

S1 S. Singh, M. Yadav, D. K. Singh, D. K. Yadav, P. K. Sonkar and V. Ganesan, *New Journal of Chemistry*, 2022, **46**, 13422–13430.

S2 P. K. Sonkar, K. Prakash, M. Yadav, V. Ganesan, M. Sankar, R. Gupta and D. K. Yadav, *J Mater Chem A*, 2017, **5**, 6263–6276.

S3 A. D. Adler, F. R. Longo, J. D. Finarelli, J. Goldmacher, J. Assour and L. Korsakoff, *J Org Chem*, 2002, **32**, 476–476.

S4 W. R. Osterloh, S. Kumar, N. Chaudhri, Y. Fang, M. Sankar, K. M. Kadish, M. Sankar and K. M. Kadish, *Inorg Chem*, 2020, **59**, 16737–16746.

S5 A. S. Bulbul, N. Chaudhri, M. Shanu, J. N. Acharyya, G. Vijaya Prakash and M. Sankar, *Inorg Chem*, 2022, **61**, 9968–9982.

S6 Y. Belghith, J. C. Daran and H. Nasri, *Acta Crystallogr*, 2012, **68**, 1104–1105.

S7 T. Zhao, C. Hou, H. Zhang, R. Zhu, S. She, J. Wang, T. Li, Z. Liu and B. Wei, *Sci Rep*, 2014, **4**, 1–7.

S8 D. K. Singh, M. N. Karuppusamy, A. Shrivastava, T. Palanisamy, I. Sinha and V. Ganesan, *ACS Catal*, 2023, **13**, 4155–4167.

S9 X. Zhang, Z. Wu, X. Zhang, L. Li, Y. Li, H. Xu, X. Li, X. Yu, Z. Zhang, Y. Liang and H. Wang, *Nat Commun*, 2017, **8**, 1–8.

S10 G. Prabhavathi, M. Arjun and R. Yamuna, *Journal of Chemical Sciences*, 2017, **129**, 699–706.

S11 A. Wang, J. Song, Z. Huang, Y. Song, W. Yu, H. Dong, W. Hu, M. P. Cifuentes, M. G. Humphrey, L. Zhang, J. Shao and C. Zhang, *Nano Res*, 2016, **9**, 458–472.

S12 M. Tasleem, M. Yadav, V. Ganesan and M. Sankar, *Langmuir*, 2023, **39**, 8075–8082.

S13 D. K. Singh, V. Ganesan, D. K. Yadav, M. Yadav, P. K. Sonkar and R. Gupta, *Catal Sci Technol*, 2021, **11**, 1014–1026.

S14 Q. Zuo, G. Cheng and W. Luo, *Dalton Transactions*, 2017, **46**, 9344–9348.

S15 Q. Xu, L. Zhao, R. Yuan, Y. Chen, Z. Xue, J. Zhang, X. Qiu and J. Qu, *Colloids Surf A Physicochem Eng Asp*, 2021, **629**, 127435–127444.

S16 Y. Wei, L. Zhao, R. Yuan, Z. Xue, J. Mack, C. Chiyumba, T. Nyokong and J. Zhang, *Inorg Chem*, 2022, **61**, 13085–13095.